

=====

Petrological, mineralogical and geochemical studies of Late Ediacaran A-type volcanics, North Arabian Shield, Saudi Arabia

Shehta E. Abdullah¹, Waheed I Elwan¹, Mohamed M. Abu Anbar², Sayed A.

Azzaz¹, Khuloud N. Alrashidi³, Amr El-Awady¹

¹Geology Department, Faculty of Science, Zagazig University, Zagazig, Egypt

²Geology Department, Faculty of Science, Tanta University, Tanta, Egypt

³Ministry of Education - State of Kuwait

Abstract: The Late Ediacaran A-type alkaline Jabal Asfar Thwelil volcanics (JATV) represent the ultimate episode in the Precambrian growth of the Arabian Shield. This episode is characterized by switching the geodynamic regime from subduction-related to post-collision and intra-plate extension. JATV are exclusively subaerial and unmetamorphosed volcanics that are represented by porphyritic rhyolite, aphyric rhyolite and deposition of pyroclastics and ignimbrites. The fall out pyroclastics include fine (ash) tuffs, banded tuffs, crystal tuffs and lithic tuffs. Geochemically, JATV are highly evolved alkaline volcanics of comenditic rhyolitic composition. They are mainly metaluminous to slightly peralkaline domains similar to the trend of Pan-African peralkaline granites. JATV are belonging to A-type ferroan alkaline magma, which were emplaced during an anorogenic stage during extensional stresses and intraplate rifting. The porphyritic rhyolite and aphyric rhyolite are cogenetic. The present data suggests the generation of parental magma through partial melting of asthenospheric mantle sources, which subsequent followed by extensive fractional crystallization. The main fractionated phases were feldspars, apatite and Fe-Ti oxide. The suggested source of JATV was low oxygen fugacity hot-dry- reduced magma of asthenospheric mantle source. This source was garnet-free and spinel-rich source and comprising a crustal component. This crustal component may either recycled component from pre-collision event or a recycled component in the source. The ANS was subjected to intensive lithospheric delamination subsequent to slab break-off and crustal/mantle thickening result from the collision between East and west Gondwana. During the late post-collisional crustal extensional stage (590-550 Ma), the upper mantle-derived melts produced in turn as a result of decompressional melting due to erosional uplifting and consequently this alkaline/peralkaline mantle-derived melt intraplate the lower/middle crustal levels. This intraplate process is facilitated by the strike-slip faults and shear zones (e.g. Shammar shear) and consequently this melt either form A-types plutonic (i.e. the associated alkali granite) complexes or continue to arrive as shallow crustal magma to form JATV. The JATV rocks were subjected to intense faulting and shearing (i.e. belong to Shammar shear), which result in metasomatic alterations (illitization, hematitization and sericitization) along these faults and shear zones. These alteration zones contain promising source for U and Zr mineralizations, which may be formed by supergene or low-temperature post-magmatic hydrothermal phase especially along faults or brecciated shear zones, characterized by strong alteration, where the precipitation of U, Zr- bearing minerals occurred as the residual late hydrothermal fluids cool to the temperature of meteoric water.

Date of Submission: 23-08-2022

Date of acceptance: 21-09-2022

I. Introduction

The Arabian-Nubian Shield (ANS) represents juvenile continental crust that was exposed around the Red Sea flanks in Saudi Arabia, Eastern Desert and Sinai in Egypt, Red Sea Hills of Sudan and reach south to Eritrea and Ethiopia. It was evolved between ~870-550 Ma and considered as one of the largest tracts of juvenile continental crust of Neoproterozoic age on Earth (e.g., Patchett & Chase, 2002). ANS documents Neoproterozoic tectonics bracketed by two supercontinent cycles, namely the fragmentation of Rodina and

amalgamation of Gondwana (Johnson et al., 2011). The ANS stabilization occurred in mid-Cambrian times (~520 Ma) and was exhumed in Neogene time as a consequence of Red Sea rifting. The Red Sea Rift started ~30 million years ago, leading to the separation of the Africa from Arabian plate, stretching about 2000 km from NNW to SSE (Bosworth et al., 2005; Corti, 2009; Avni et al., 2012).

The ANS juvenile crust comprises metamorphosed volcano-sedimentary rocks, ophiolite suites and calc-alkaline metagabbro-diorite-granitoid rocks formed during the pre-collisional (island-arc) stage (~820–700 Ma). The collisional stage (670–630 Ma) is characterized by the abundances of weakly deformed calc-alkaline gabbros and granodiorites. The volcanics succession together with undeformed calc-alkaline granitoids and alkaline/peralkaline granitoids are formed during late- to post- collisional stage (630–580 Ma) of the ANS crust evolution (Farahat et al., 2007; 2011).

Four major volcanic episodes have been recognized in the Neoproterozoic crust of the ANS, namely; ophiolitic metavolcanics, island arc metavolcanics, calc-alkaline volcanics and alkaline/peralkaline volcanics (El Gaby, 1990; Stern et al., 1991; Mohamed et al., 2000., Samuel et al., 2007; Basta et al., 2011). Ophiolitic metavolcanics are represented by tholeiitic pillow basalts (Basta et al., 2011), while island arc metavolcanics are submarine volcanics of calc-alkaline nature and typically low in potash and comprise andesites and dacites together with subordinate basalts and rhyodacites (El Gaby, 1990; Stern et al., 1991). The calc-alkaline volcanics are exclusively subaerial, unmetamorphosed and are medium- to dominantly high-K in composition and show typical calc-alkaline characters (Mohamed et al., 2000). The alkaline volcanics were emplaced during a non-orogenic period after termination of the Pan-African orogeny (Samuel et al., 2007). They comprise alkaline/peralkaline rhyolites, commendite, pantellerite, ignimbrite and pyroclastics

The late Neoproterozoic tectono-magmatic stage of the ANS represents the development and maturation of the continental crust from orogen to crustal stabilization. The late Neoproterozoic, especially in the northern ANS, was characterized by eruptions of volcanics, deposition of molasse-type metasediments and emplacement of calc-alkaline granites (Eliwa et al., 2014; El-Bialy, 2013). Volcanosedimentary basins are common geologic feature in ANS (Fig. 1) as they occur throughout the Arabian Shield and in the northern Nubian Shield. The basin assemblages are ranging from Cryogenian to Ediacaran (i.e. 785 - 560 Ma). Depositional units within the basins may be entirely or largely volcanic or terrestrial basin (i.e. Dokhan volcanics and Hammamat sediments) or volcanoclastic terrestrial and shallow marine basin (i.e. Shammar group) in origin. Most of these basins contain volcanic assemblages of basalt, andesite, or rhyolite flows, agglomerates, ignimbrites, and tuffs. Volcanosedimentary basins in ANS are rarely overlies a forearc accretional prism, but they are commonly overlying plutonic rocks from deep in the magmatic core of the arc systems and some suture zones between amalgamated terranes (Johnson et al., 2013).

The magmatic history of the post-accretionary stage of the ANS includes two major magmatic episodes: the calc-alkaline phase (635–610 Ma) and the alkaline phase (610–580 Ma). Just close to the end of the post-collisional stage, the alkaline/peralkaline volcanic sequence erupted during a non-orogenic over a period starting from the late Ediacaran (610–590 Ma) to the early Cambrian (540 Ma). Mushkin et al. (1999) described these alkaline volcanics as small in volume, but widely scattered over the entire Shield and they relate these volcanic to a within-plate tectonic environment. These volcanics comprise alkali rhyolite, comendite and pantellerite flows, with abundant ignimbrites and pyroclastic deposits. They were erupted during a non-orogenic period in a state of tensile stress, block faulting and differential uplift. During the closing stages of this volcanic phase, large-scale caldera collapse occurred, and ring dykes were injected into the bordering fractures. The suggested models for these volcanics including active continental margin, intracontinental rift model, transition

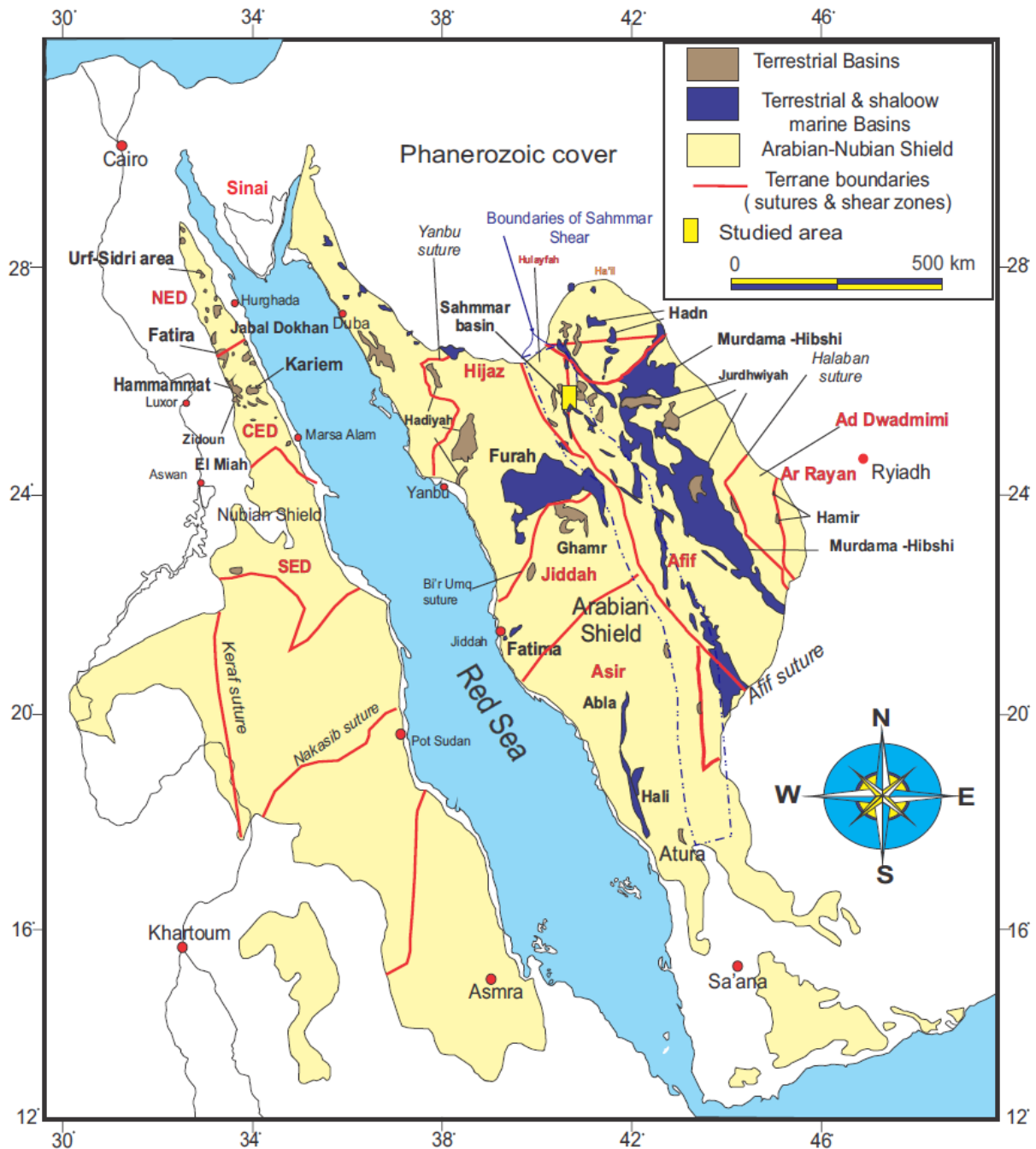


Fig. 1: Volcanosedimentary basins in the Arabian-Nubian Shield (after Johnson et al., 2011). Note: location of the studied area (i.e., red rectangle), basin names are in black and bold, while terrane names in red and bold.

between compression and extension (e.g., Abdel Wahed et al., 2010; Azer and Farahat, 2011; Be'eri-Shlevin et al., 2011; Eliwa et al., 2014; Mohamed et al., 2000). Until now, there have been no substantial studies on the alkaline/peralkaline volcanics of Neoproterozoic era in the Arabian Shield, despite the fact that other similar alkaline/peralkaline volcanics in the Nubian Shield have been studied in more detail. In this work, we provide new geological, petrographical and geochemical data on the late Neoproterozoic alkaline/peralkaline felsic volcanics exposed in the Jabal Asfar area. This is done to examine the genetic relationships between different components of the alkaline/peralkaline volcanics and to provide geochemical constraints on the nature of the magma source, geotectonic affinity, magma source, metasomatic alteration and geodynamic evolution during the post-collisional stage in the ANS of late Ediacaran A-type JATV.

II. Geologic setting

JATV is located approximately 200 km southwest of the regional center of Ha'il area, in the north-central part of Saudi Arabia, and ~ 8 km to the east of Al-Ha'it City (Fig. 2). JATV took its name from Asfar, which mean 'yellow color' describing the yellow color alteration halos (i.e., oxidation to limonite and/or U-mineralizations) and Thwelil is the name of an old village.

The exposed rock units in the study are of Late Proterozoic rocks and Cenozoic volcanics, the latter belong to Harrat Khaybar. The late Proterozoic rocks include Hulayfah Group and Shammar group. The area is crosscut by faults trending NW-SE and NE-SW (Fig. 4) these faults belong to Shammar shear zones. The oldest Late-Proterozoic rocks being the Hulayfah Group composed mainly of mafic and intermediate volcanics and associated sediments, all of which are underwent polyphase folding and metamorphism to greenschist grade (Johnson, 2006).

Shammar group is restricted to the northern part of Arabian Shield, and it is unconformably overlies the Hulayfah group, which has an age between (800–690 Ma; Hadley and Schmidt, 1980). According to Kemp (1998), Shammar group was evolved in extensional continental basins forming after the cratonization of the Arabian Shield. Shammar basins were infilled with acidic flows, pyroclastics (mainly ignimbrite). Shammar group rocks intrude a suite of acidic intrusive tonalite-granodiorite suite (~ 738 Ma; Quick and Doebrich, 1987), while they intruded by alkaline granites and granophyres (575-580 Ma; Stuckless et al., 1984) and unconformably overlain by Harrat volcanics (i.e., Cenozoic basalt and rhyolite). Shammar group and alkali-granites and gnophyres are probably the products of intracontinental magmatism (Kemp, 1998).

The studied alkaline volcanics are belonging to Shammar group, which represents the latest volcanic activity in the Arabian Shield. JATV forms domal-shaped mass (~ 1120 m above Sea Level), that cover an area of ~ 10 km² and bounded by latitudes 25° 58' 36'' and 25° 59' 44.16'' N. and longitude 40°32'22.56'' and 40°34'6.24'' E (Fig. 3 & 4).

JATV contains acidic flows, pyroclastics (mainly ignimbrite) and reworked volcanics, caldera and lava domes. JATV contains a rhyolitic dome on the edge of a volcanic caldera, which is filled with partially reworked ignimbrites with an age ~ 572 Ma (Hadley and Schmidt, 1980). The massive porphyritic rhyolite outcrops at the central part of this dome (Fig. 5a & b), representing the nucleus of these volcanic rocks. Porphyritic rhyolite is highly jointed and show columnar structure (Fig. 5b). Along fault planes the studied porphyritic rhyolite affected by metasomatic alteration (Fig. 5c) as they show ferruginous alteration (i.e., hematite-goethite-limonite) in many parts. JATV rocks are commonly sheared and show cataclastic effects. They are mainly viscous acidic lavas showing foliation (Fig. 5d) of flow folding. Along the strike toward the rhyolite dome, acidic volcanic tuffs, which upon weathering change to white tuffs enclosing flow rhyolite boulders and agglomerate (Fig. 5e). At the edge of the caldera, thin layers of green tuffs enclosing large quantities of boulders are encountered. Many quartz and chalcedony veins are recorded; the thickest one is that located to the southwest of the dome that cut across Jabal Ashkar Thwelil (Fig. 5f). These veins are mostly trending NW-SE and rarely trending in NS, NE-SW directions. Chalcedony veins show alteration halos with different colors, dark brown to black halos as indication of hematite-goethite oxidation (Fig. 6a), reddish yellow halos as indication on limonite-hematite oxidation and yellow halos could be indications of the presence of U-mineralizations. Fluorite-uranium mineralized veins are commonly scattered in the flow rhyolite. Most of the western part of the study area is covered by the Cenozoic alkali basalts and rhyolites of the extensive Harrat Khaybar lava field (Figs. 2, 3 & 4), with some scattered inliers of Precambrian rocks separated from the basalts by terrace deposits (mainly gravel, sandy clays and gypsum).

III. Petrography

The studied volcanics are subdivided into rhyolitic lavas (aphyric and porphyritic rhyolites), sheared rhyolitic, pyroclastics (fine tuffs, banded tuffs, crystal tuffs and lithic tuffs) and ignimbrite. Beside these rock types of the chalcedony veins are studied petrographically. The detail petrographic description of different rock types is given hereinafter.

3.1. Porphyritic rhyolite

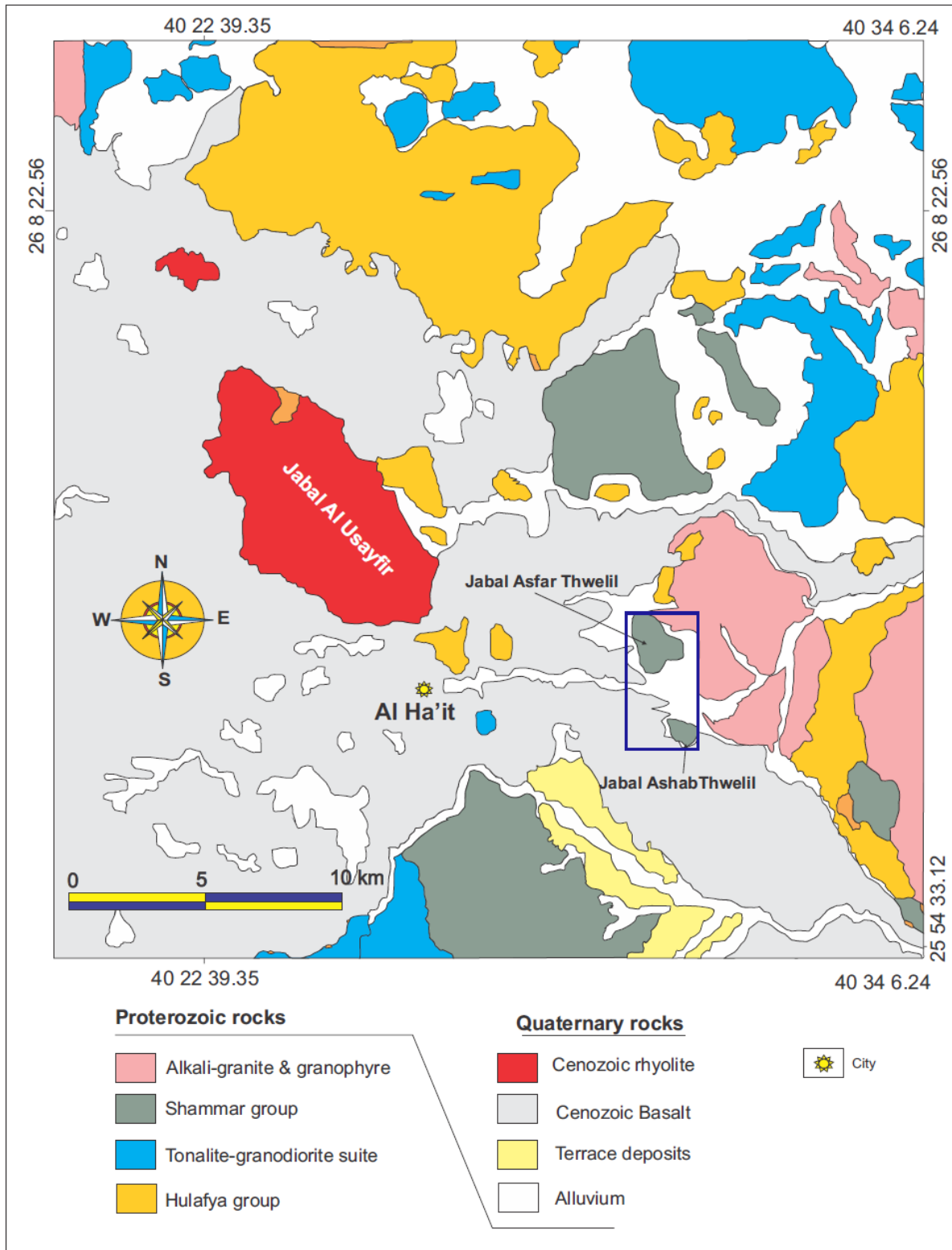


Fig. 2: Geological map of the Al Ha'it area (modified after Al-Anazi, and Al-Saleh, 2013).

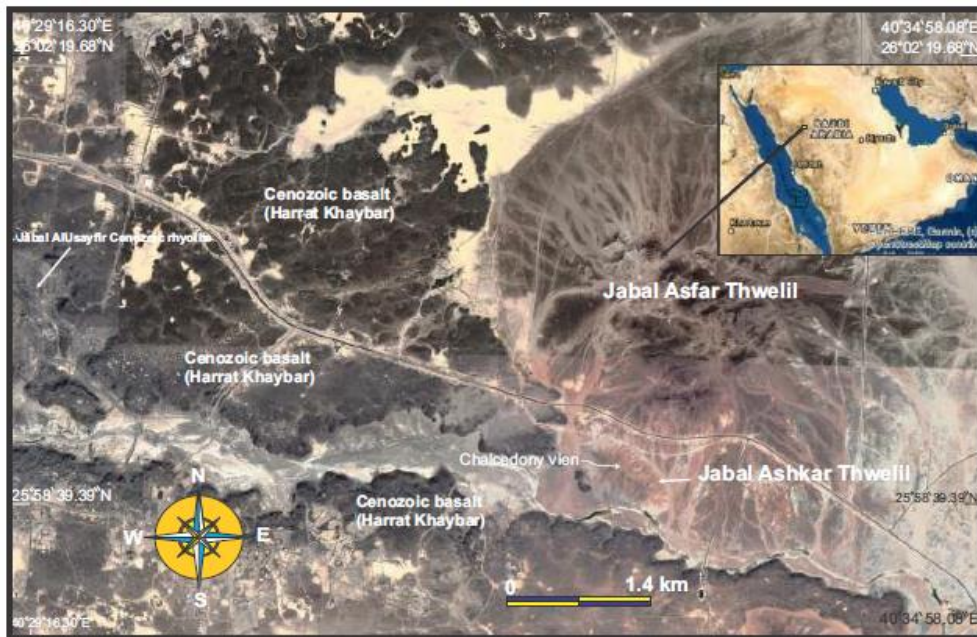


Fig. 3: Google Earth map of JATFV, Saudi Arabia.

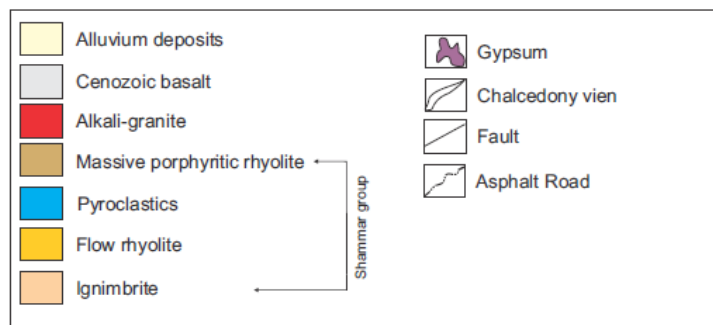
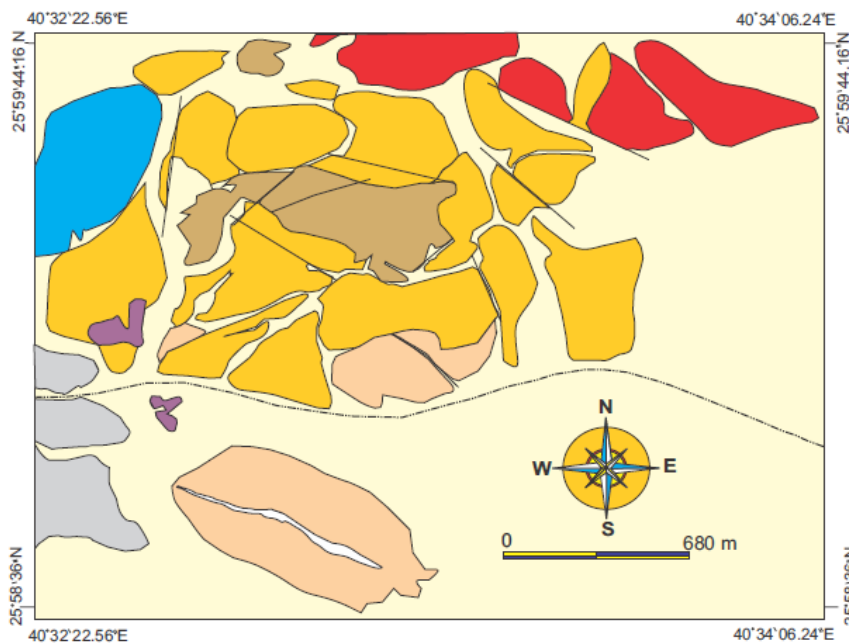


Fig. 4: Detailed geological map of the Jabal Asfar Thwelil volcanics.

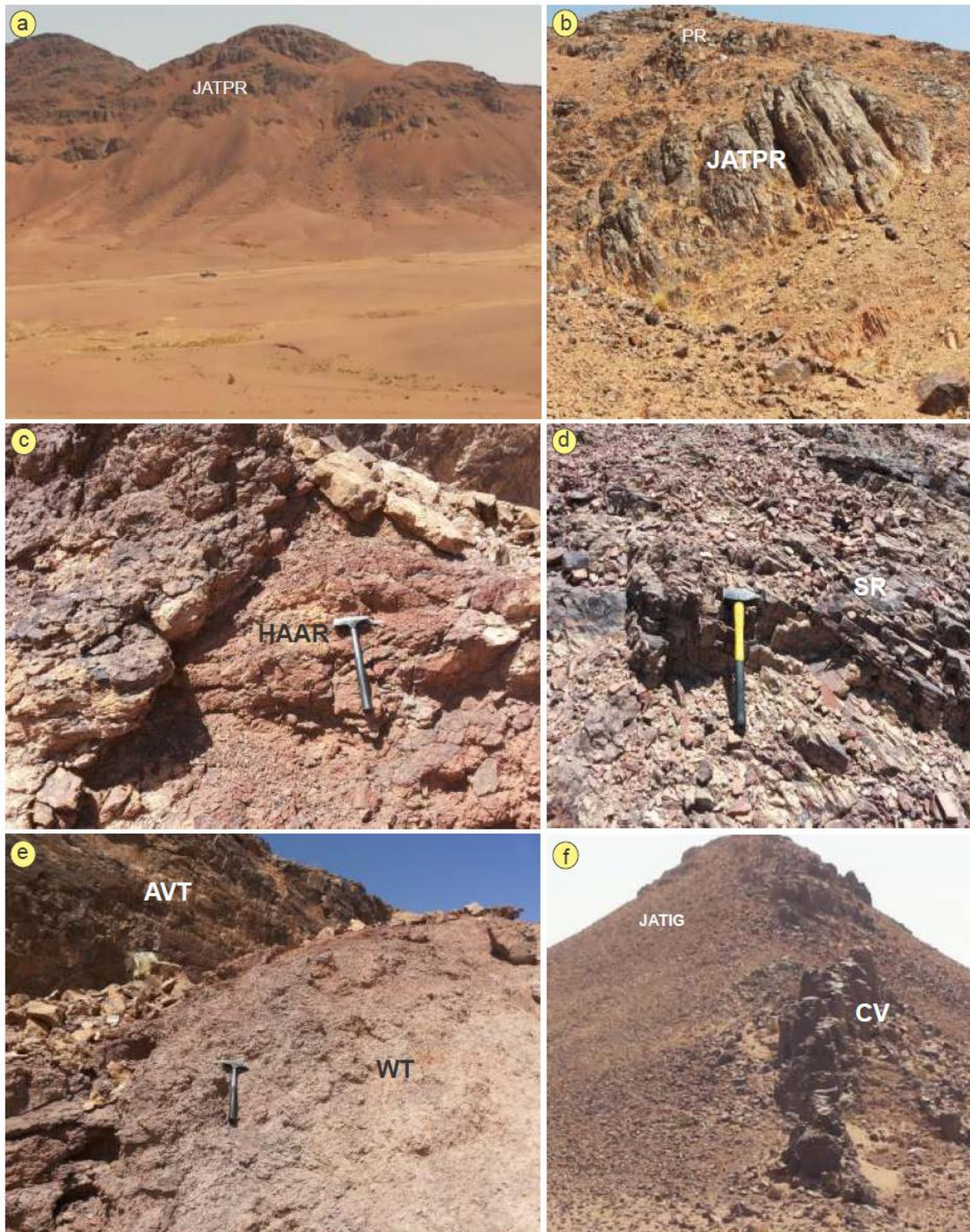


Fig. 5. Field photos of JATV showing, a) General view of Jabal Afar Thwelil porphyritic rhyolite (JATPR); b) Highly jointed porphyritic rhyolite core altered by weathering; c) HAAR; d) Sheared rhyolite (SR) showing foliation; e) Acidic volcanic tuffs (AVT) altered to white tuffs (WT) enclosing flow rhyolite boulders and agglomerate; f) Jabal Ashkar Thwelil ignimbrite (JATIG) to south of Jabal Asfar Thwelil, which is cut by chalcodony vein (CV). Porphyritic rhyolite is rather similar to aphyric rhyolite in composition, but commonly contains higher amounts of phenocrysts that may constitute 20-50 vol. % of the rock. Moreover, the porphyritic rhyolite possesses coarser grained groundmass than aphyric rhyolite. The phenocrysts are represented mainly by K-

feldspar and quartz with rare albite embedded in a microcrystalline felsic groundmass (Fig. 6b). The groundmass consists essentially of K-feldspars and quartz exhibiting granophyric and micrographic textures. K-feldspar phenocrysts form anhedral to subhedral crystals usually showing simple twinning. Some K-feldspar phenocrysts are corroded and embayed by the groundmass (Fig. 6b). Quartz occurs as subhedral to anhedral porphyritic crystals or intergrown with K-feldspar developing granophyric and micrographic textures.

3.2. Aphyric rhyolite

Aphyric rhyolite represents the most common rock type among the volcanic rocks of JATV. It is fine-grained and consists essentially of K-feldspar and quartz together with rare albite. The aphyric rhyolite showing various textures, including micrographic and spherulitic textures (Fig. 6c). The spherulites may develop at widely spaced centers or occur as a mass of coalescing spherulites (Fig. 6c). They are composed of radial fibers of K-feldspar and quartz; the center is sometimes formed of fine equant crystals of quartz. Spherulites are found in the form of spherical, fan (Fig. 6c) and axiolitic types. The flow line and structures around the spherical spherulites pass undisturbed through spherulites (Fig. 6c), indicating that the spherulites grew after development of the flow structures, probably in solid glass (devitrification). Many of aphyric rhyolites samples are recorded in few samples. Some aphyric rhyolite samples K-feldspars contain minute microphenocrysts of quartz and alkali feldspars and glass (Fig. 6d) are highly altered and showing resorption features, especially near the shear zones.

3.5. Sheared rhyolite

The sheared rhyolite represents core samples collected from the shear zones. It has the same composition of aphyric rhyolite (Fig. 6e) and consists essential of K-feldspars and quartz. The groundmass, which is consisting mainly of k-feldspar and quartz grains commonly show cataclastic and shearing effects (i.e. mylonitic texture and rotation; Fig. 6e). Feldspar show high degrees of argillic (i.e. kaolinitization and/or illitization) and sericitization (Fig. 6f). Many veins of secondary carbonate and quartz are observed cutting through the rock.

3.3. Pyroclastics

Pyroclastics differ from the rhyolitic lavas by their pyroclastic texture. They include fine tuff, banded tuff, crystal tuffs and lithic tuffs. Fine tuff consists of very fine-grained vitreous-ashy material with tiny particles of quartz and feldspars. Locally, it is cutting by secondary veins of quartz and carbonates. Banded tuff is very fine grained and composed of alternating laminae and thin beds of vitreous-ashy material of variable colours. Tiny particles of quartz, feldspars and mafics are abundant and embedded in a sericite-rich groundmass.

Crystal tuffs are composed mainly crystal fragments. The crystal fragments are represented by quartz and K-feldspars with rare albite, mafics and opaques, which are embedded in vitric or fine tuffaceous groundmass (Fig. 7a). Quartz occurs as angular to subrounded fractured crystal fragments. These fractures are eventually allowing the crystal to separate into fragments. Quartz shows micropoikilitic texture micropoikilitic texture (Fig. 7b). K-Feldspar crystal fragments are also angular and show slight alteration to sericite. Rare angular lithic fragments of rhyolitic composition are recorded.

Lithic tuff is poorly sorted and composed of rock fragments with minor crystal and glass fragments. Rock fragments are angular to subangular in shape. They are rhyolitic to trachytic in composition (Fig. 7c). The crystal fragments are represented by quartz and K-feldspars. The glass fragments are rarely devitrified. The rhyolitic rock fragments consist essentially of quartz and highly altered K-feldspars. The trachytic rock fragments show trachytic texture (Fig. 7c) and consist mainly of albite with less amounts of quartz and altered mafic minerals.

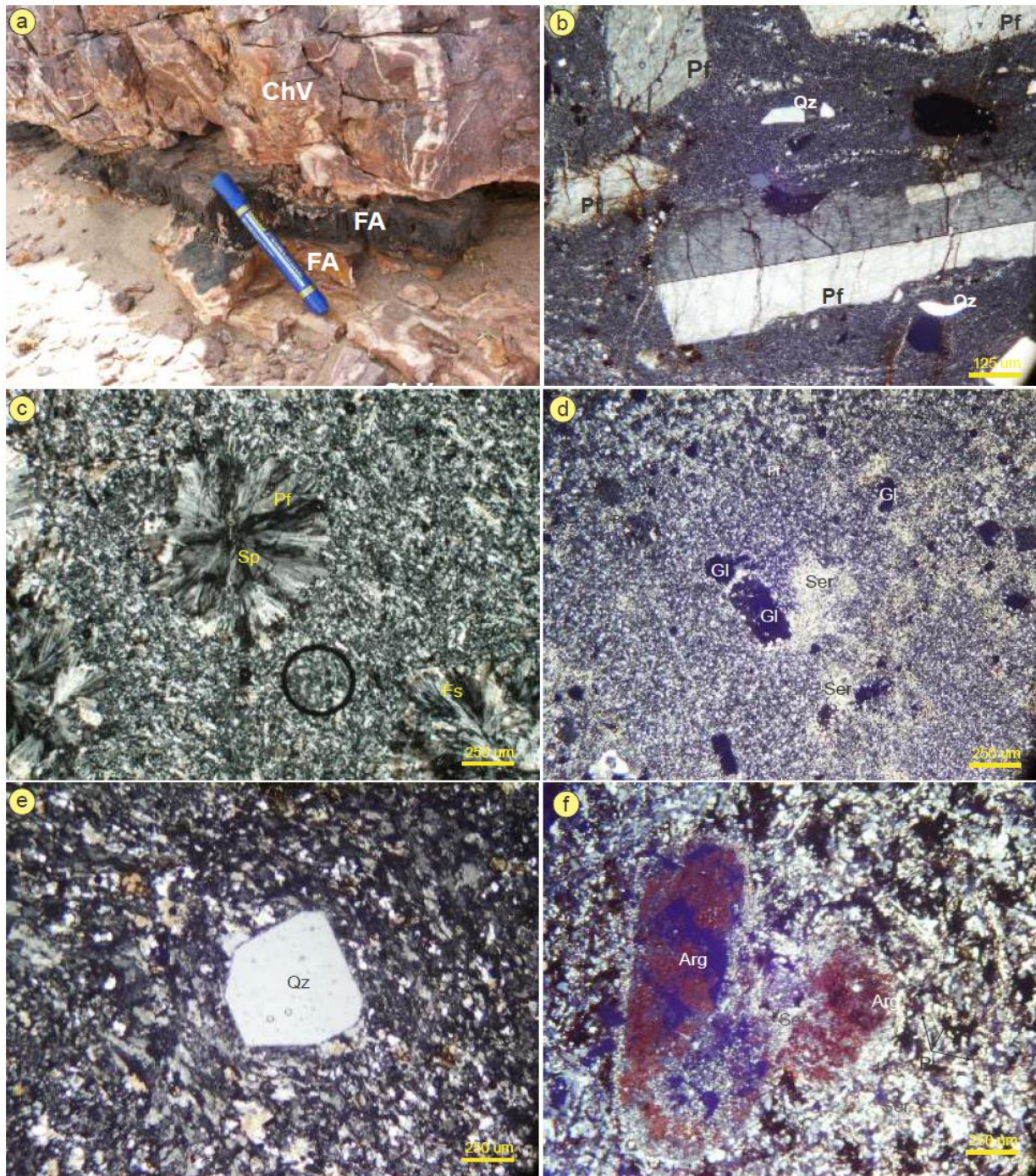


Fig. 6. Field photos (a) and Photomicrographs (b-f) of JATV showing, showing, a) Chalcedony vein (ChV) associated by ferruginous (hematite-goethite) alterations (FA); b) Porphyritic rhyolite showing large K-feldspar phenocrysts (Pf) and smaller quartz grains corroded and embayed by fine groundmass from quartz and K-feldspar and albite, CN; c) Aphyric rhyolite showing spherical (Sp) and fan-shaped (Fs) spherulites, where the flow line and structures pass undisturbed through spherulites, CN; d) HAAR showing fine grains of altered K-feldspar (Pf), quartz (Qz) and glass (Gl), which are embedded in a sericite-rich groundmass, CN; e) Sheared rhyolite contains embayed dipyramid Quartz phenocryst (Qz) in finer groundmass of quartz and K-feldspar. The groundmass quartz grains show cataclastic and shearing effects (i.e. mylonitic texture and rotation), CN; f) Sheared rhyolite showing strong argillic alteration (illitization or kaolinitization).

3.4. Ignimbrite

The ignimbrite is rhyolitic in composition and show regular orientation of crystal fragments and flattened glass particles (fiamme) embedded in a tuffaceous groundmass. The crystal fragments include quartz and K-feldspars. The fiamme is flattened and formed of stained glassy material. Sometimes, the thin fiamme are gently curved around crystal fragments. The groundmass shows fluidal foliations around the crystal fragments (Fig. 7d) and formed of acid volcanic glass and glass shards of irregular shape. The matrix is commonly shows faint axiolitic strands and faint eutaxitic texture (i.e. wrapping around crystals and lithic fragments)

3.6. Chalcedony

Chalcedony is a cryptocrystalline variety of silica. It is massive and invaded by coarse quartz veins showing coarse comb textures (Fig. 6e). Coarse quartz represents multiple generations of secondary quartz that have crystallized in fractures, generally as a result of shearing. Ferruginous alteration is associated with chalcedony vein (Fig. 7f).

IV. Geochemistry

4.1. Analytical methods

Based on the petrographic studies, twenty-two representatives rock samples (4 samples from porphyritic rhyolite, 6 from aphyric rhyolite, 8 from hydrothermally altered aphyric rhyolite (HAAR), 2 from sheared rhyolite and 2 from chalcedony vein) were analysed for major, trace, and rare earth elements (Table 1, 2, 3). The analyses were carried out at the State Key Laboratory of Continental Dynamics, Northwest University, Xian in China. The analytical procedures for major elements were as follows: 0.7g sample powders were mixed with 3.6 g $\text{Li}_2\text{B}_4\text{O}_7$, 0.3 g LiF, 0.4 g NH_4NO_3 and 2-3 drops 1.5% (w/w) LiBr solution. The mixture was put into a platinum (Pt 95%+Au 5%) crucible and melted in a high frequency melting instrument into a glass disk before analysis. Then the glass beads were analyzed by XRF (Rigku RIX2100). For trace elements analyses: 50 mg sample powders were digested using HNO_3 , HF and HClO_4 in polytetrafluoroethylene (PTFE) bombs with steel sleeves heated with an electronic oven at 190 °C for 48 hours. The final solutions, diluted to 80 g using 2% HNO_3 with internal standard (10 ng/g Rh in the solution), were analyzed using ICP-MS (Agilent 7500a). Analyses of USGS rock standards (BCR-2, BHVO-1, and AVG-1) indicate that the precision and accuracy are better than 5% for major elements and 10% for trace elements. The detailed analytical procedures were shown in Liu et al. (2014).

4.2. Geochemical characteristics

Geochemistry of the JATV was largely neglected. There are no geochemical data available on these volcanics. The results of chemical analyses (major oxides, trace elements and REEs.) of lava flows, sheared rhyolite and chalcedony are represented in tables (1, 2, 3). The chemical composition of the studied JATV compared to the averages of the published data on other felsic volcanics from ANS (e.g. El-Baily et al., 2022; Samuel et al., 2007), averages of A-type granites and averages of the continental crust (Tables 1, 2). The analyzed samples of lava flows are acidic in composition. The silica contents of the analyzed volcanic samples cover a wide range of compositions (70.38-80.22 wt. %) and differentiation indices ($\text{DI} = 96.46\text{-}81.63$ %). Also, they show wide variation in the contents of alkalis (K_2O and Na_2O) in some of the analyzed rocks, especially aphyric rhyolites, due to K-metasomatism (Table 1). The analyzed chalcedony samples have high silica contents (92.82-92.97 wt. %) with narrow variation and much depleted in other major oxides comparing with the volcanic rocks.

The contents of the analyzed trace elements show wide variations (Table 2). The analyzed volcanics have low contents of Ba, Sr, Cr, V, Ni and Cu, but they have high contents of Nb, Y, Zr, Hf, Th, Co, Ga, Ta and U. Abnormal concentrations of Zr (81668-90010 ppm), Nb (538-1719 ppm), Hf (1274-1554 ppm), U (569-1512 ppm) are recorded in the core samples of the sheared rhyolite. Chalcedony veins are much depleted in all trace elements. The variation diagrams of the JATV are not plotted because they are very scattered due to affect of different types of alteration such as silicification, illitization and sericitization.

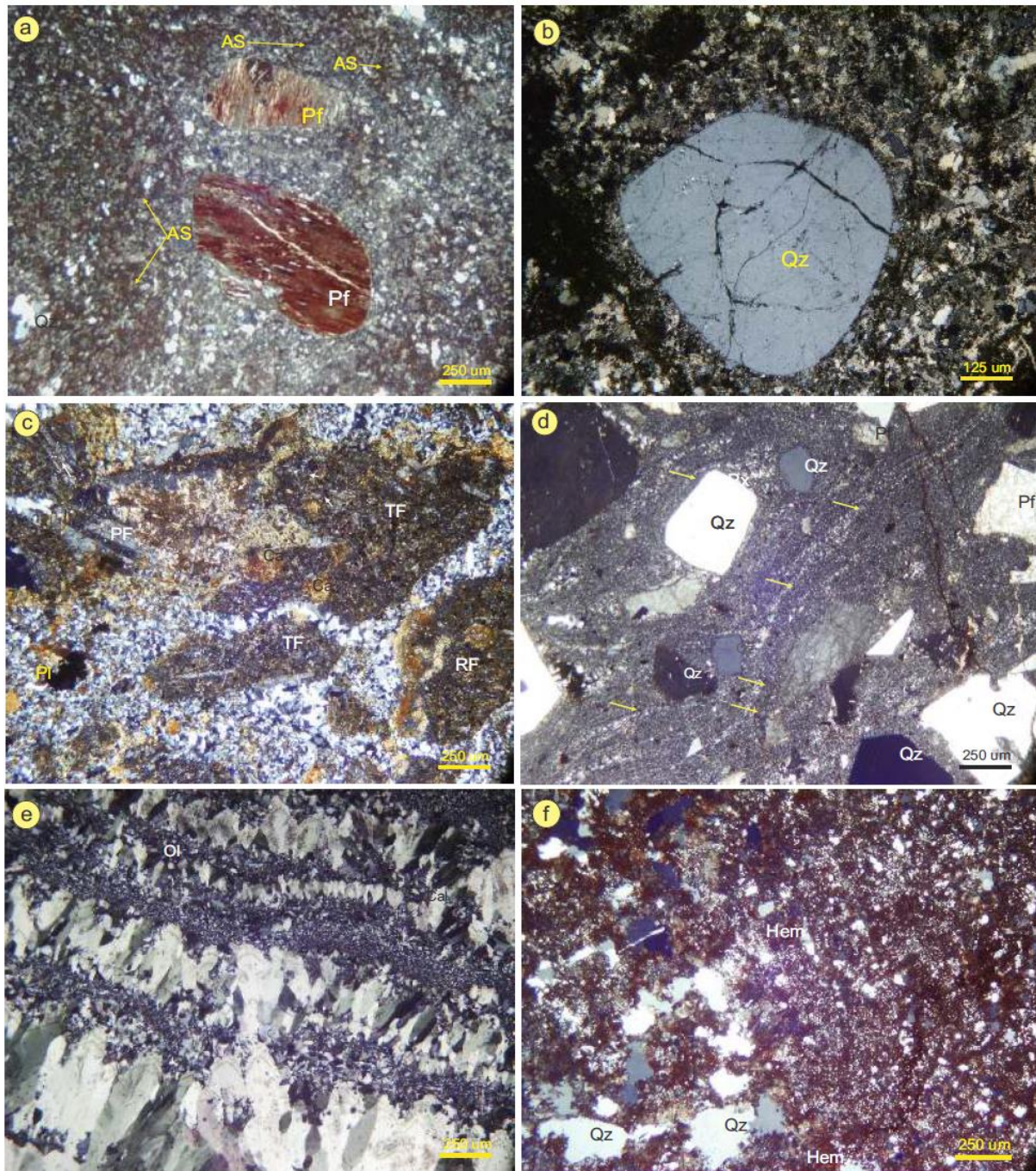


Fig. 7. a) Photomicrographs of JATV showing, a) Crystal tuff showing K-feldspar fragments (Pf) settled in tuffaceous groundmass, which has internal banding, faint axiolitic strands (AS) and micro-poikilitic texture, CN; b) Crystal tuff showing a large embayed fractured subrounded quartz crystal (Qz). Fractures eventually allow the crystal to separate into fragments. Quartz showing micropoikilitic texture. CN; c) Lithic tuff showing crystal fragments of plagioclase (Pl) and rock fragments trachyte (TF) and rhyolite (RF) settled in fine groundmass of quartz and calcite (Ca) crystals. Trachytic fragment shows microtrachytic texture, CN; d) slightly welded ignimbrite fine patchy matrix that has splotchy quartz growths. The matrix shows faint axiolitic strands and faint eutaxitic texture, CN; e) Chalcedony vein showing comb-texture, which is consisting of coarse quartz represents multiple generations of secondary quartz that have crystallized in fractures, CN; f) Ferruginous alteration (i.e. hematite) is commonly associated with chalcedony vein.

Table 1. Major oxide contents and calculated normative compositions of Jabal Asfar Thwelil volcanics, Saudi Arabia.

Rock type	Fresh porphyritic rhyolite				Fresh aphyric rhyolite						Hydrothermal altered aphyric rhyolite			
Sample No.	S20	S21	S22	S23	S18	S26	S38	S39	S42	S46	Average	S9	S15	S19
Major oxides (wt.%)														
SiO ₂	75.99	75.66	77.52	77.88	78.95	75.41	75.09	74.93	74.88	75.33	76.16	79.73	75.79	75.33
TiO ₂	0.18	0.20	0.19	0.19	0.09	0.13	0.12	0.12	0.14	0.13	0.15	0.09	0.14	0.09
Al ₂ O ₃	11.27	11.29	11.18	11.27	10.69	11.52	10.98	11.12	11.17	11.19	11.17	9.69	11.32	11.77
Fe ₂ O ₃	2.41	2.62	1.66	1.51	1.45	3.35	2.61	3.87	3.52	4.05	2.71	3.13	2.96	2.42
MnO	0.04	0.05	0.01	0.01	0.01	0.01	0.21	0.01	0.03	0.01	0.04	0.06	0.02	0.09
MgO	0.11	0.22	0.12	0.09	0.18	0.23	0.28	0.18	0.14	0.09	0.16	0.34	0.17	0.12
CaO	0.50	0.60	0.32	0.12	0.15	0.25	0.49	0.32	0.29	0.21	0.33	1.04	0.31	0.57
Na ₂ O	3.27	3.01	2.17	2.70	0.18	1.64	4.28	4.13	4.14	3.99	2.95	0.16	3.44	0.22
K ₂ O	4.82	4.76	5.29	5.71	6.66	5.11	4.34	4.10	4.71	3.97	4.95	3.01	4.11	7.12
P ₂ O ₅	0.01	0.03	0.01	0.01	0.04	0.02	0.03	0.01	0.01	0.01	0.02	0.03	0.01	0.02
LOI	1.03	1.33	1.33	0.68	1.41	2.18	1.91	0.71	0.52	0.63	1.17	2.65	1.52	2.26
Total	99.63	99.77	99.80	100.16	99.81	99.85	99.89	99.50	99.55	99.61	99.76	99.93	99.79	100.01
Normative composition														
Quartz	36.76	37.7	43.74	39.51	52.06	44.82	33.31	33.04	32.1	34.6	-	64.78	38.31	45.18
Corundum	-	0.17	1.34	0.45	3.06	2.96	-	-	-	-	-	4.48	0.68	2.78
Orthoclase	28.95	28.64	31.79	33.96	40.04	31.01	26.11	24.61	28.2	23.8	-	18.33	24.78	43.13
Albite	28.12	25.93	18.67	22.99	1.55	14.25	32.88	34.88	31.6	34.2	-	1.4	29.69	1.91
Anorthite	1.86	2.83	1.55	0.53	0.49	1.14	-	-	-	0.9	-	5.12	1.5	2.76
Acmite	-	-	-	-	-	-	1.31	0.53	1.62	-	-	-	-	-
Na-Metasilicate	-	-	-	-	-	-	0.58	-	0.47	-	-	-	-	-
Diopside	0.53	-	-	-	-	-	1.98	1.36	1.23	0.08	-	-	-	-
Hypersthene	2.83	3.63	2.09	1.78	2.17	4.74	3.51	4.69	4.49	5.19	-	4.9	4.04	3.43
Magnetite	0.58	0.64	0.41	0.37	0.34	0.78	-	0.62	-	0.92	-	0.74	0.69	0.58
Ilmenite	0.35	0.39	0.37	0.36	0.17	0.25	0.23	0.23	0.27	0.25	-	0.18	0.27	0.18
Apatite	0.02	0.07	0.02	0.02	0.09	0.04	0.07	0.02	0.02	0.02	-	0.07	0.02	0.04
Some parameters and geochemical ratios														
K ₂ O/MgO	43.82	21.64	44.08	63.44	37.00	22.22	15.50	22.78	33.64	44.11	34.82	8.85	24.18	59.33
Total Alkali	8.59	8.37	7.78	8.53	6.99	7	9.11	8.55	9.14	8.17	8.22	4.21	7.86	7.91
(Na ₂ O + K ₂ O)/CaO	16.18	12.95	23.31	70.08	45.60	27.00	17.59	25.72	30.52	37.90	30.69	3.05	24.35	12.88
K ₂ O/Na ₂ O	1.47	1.58	2.44	2.11	37.00	3.12	1.01	0.99	1.14	0.99	1.68	18.81	1.19	32.36
Mg#	8.29	14.26	12.53	10.56	19.74	11.97	17.53	8.44	7.30	4.22	11.48	17.71	10.22	8.95
AI	0.94	0.90	0.83	0.94	0.70	0.71	1.07	1.01	1.07	0.97	0.91	0.36	0.89	0.69
T Al-Ti °C*	902.5	915.2	910.1	909.1	817.6	857.8	853.6	851.9	872	862	875.1	831.4	869.9	803.8
r1	-3.80	-3.80	-4.18	-2.69	-3.07	-2.49	-2.87	-3.80	-4.18	-2.69	-3.36	-2.87	-3.80	-4.18
r2	-6.69	-6.69	-6.57	-5.16	-5.64	-5.01	-4.78	-6.69	-6.57	-5.16	-5.90	-4.78	-6.69	-6.57

Table 1. Continue

Rock type	Hydrothermal altered aphyric rhyolite					Sheared rhyolite		Calcedony veins		AB	NES	A-typeG	CC	NES	A-typeG	CC
Sample No.	S28	S29	S31	S44	S45	S27	S34	S59	S59R							
Major oxides (wt.%)																
SiO2	80.22	77.71	76.84	74.51	74.9	77.62	70.38	92.97	92.82	74.6	72.6	73.8	59.1	72.6	73.8	59.1
TiO2	0.13	0.12	0.13	0.14	0.21	0.17	0.14	0.18	0.18		0.36	0.26	0.7	0.36	0.26	0.7
Al2O3	11.09	11.26	11.19	10.57	11.44	12.56	10.49	3.25	3.28	12.8	12.1	12.4	15.8	12.1	12.4	15.8
Fe2O3	2.57	1.62	2.66	5.74	2.59	1.86	8.61	0.92	0.93	2.13	3.64	2.82	6.6	3.64	2.82	6.6
MnO	0.02	0.01	0.01	0.02	0.02	0.07	0.04	0.06	0.06	0.05	0.22	0.06	0.11	0.22	0.06	0.11
MgO	0.12	0.14	0.07	0.23	0.13	0.02	0.09	0.21	0.21	0.19	0.9	0.2	4.4	0.9	0.2	4.4
CaO	0.10	0.28	0.08	0.20	0.44	0.39	0.3	0.19	0.19	0.56	0.99	0.75	6.4	0.99	0.75	6.4
Na2O	0.10	0.22	2.64	4.39	4.27	0.13	0.23	0.08	0.09	3.56	2.34	4.07	3.2	2.34	4.07	3.2
K2O	3.25	6.68	4.74	2.60	4.63	2.9	5.82	0.59	0.59	5.93	6.6	4.65	1.9	6.6	4.65	1.9
P2O5	0.01	0.01	0.02	0.03	0.02	0.17	0.22	0.05	0.05	0.02	0.25	0.04	0.2	0.25	0.04	0.2
LOI	2.14	1.65	1.20	1.09	1.64	3.89	3.68	1.30	1.28	-	-	-	-	-	-	-
Total	99.75	99.70	99.57	99.52	100.3	99.78	100	99.80	99.68	-	-	-	-	-	-	-
Normative composition																
Quartz	67.19	50.29	41.26	35.84	32.01	67.27	43.62	90.69	90.6	-	-	-	-	-	-	-
Corundum	7.44	3.25	1.63	0.24	-	9.3	3.96	2.29	2.3	-	-	-	-	-	-	-
Orthoclase	19.72	40.31	28.36	15.69	27.79	17.9	35.98	3.54	3.55	-	-	-	-	-	-	-
Albite	0.87	1.9	22.61	37.92	33.57	1.15	2.04	0.69	0.77	-	-	-	-	-	-	-
Anorthite	0.44	1.35	0.27	0.81	-	0.86	0.06	0.63	0.63	-	-	-	-	-	-	-
Acmite	-	-	-	-	1.24	-	-	-	-	-	-	-	-	-	-	-
Na-Metasilicate	-	-	-	-	0.4	-	-	-	-	-	-	-	-	-	-	-
Diopside	-	-	-	-	1.83	-	-	-	-	-	-	-	-	-	-	-
Hypersthene	3.45	2.24	4.94	7.83	2.69	2.29	11.54	1.44	1.46	-	-	-	-	-	-	-
Magnetite	0.61	0.39	0.61	1.31	-	0.48	2	0.26	0.26	-	-	-	-	-	-	-
Ilmenite	0.25	0.23	0.25	0.27	0.41	0.34	0.28	0.35	0.35	-	-	-	-	-	-	-
Apatite	0.02	0.02	0.04	0.07	0.04	0.39	0.5	0.11	0.11	-	-	-	-	-	-	-
Some parameters and geochemical ratios																
K2O/MgO	27.08	47.71	67.71	11.30	35.62	145	64.67	2.81	2.81	-	-	-	-	-	-	-
Total Alkali (Na2O+K2O)/CaO	3.45	7.18	7.46	7.19	9.34	3.42	6.35	0.86	0.87	-	-	-	-	-	-	-
K2O/Na2O	33.50	24.64	92.25	34.95	20.23	7.77	20.17	3.53	3.58	-	-	-	-	-	-	-
Mg#	32.50	30.36	1.80	0.59	1.08	22.31	25.30	7.38	6.56	1.67	2.82	1.14	0.59	-	1.14	0.59
AI	8.47	14.62	4.96	7.35	9.04	31.14	30.91	2.09	2.03	-	-	-	-	-	-	-
AI	0.33	0.67	0.85	0.95	1.05	0.27	0.64	0.24	0.24	-	-	-	-	-	-	-
T Al-Ti °C*	862.9	850.2	861.7	878.8	919.5	881.6	879.8	1042	1041	-	-	-	-	-	-	-
r1	-2.69	-3.07	-2.49	-2.87	-3.80	-3.07	-2.49	-4.18	-2.69	-	-	-	-	-	-	-
r2	-5.16	-5.64	-5.01	-4.78	-6.69	-5.64	-5.01	-6.57	-5.16	-	-	-	-	-	-	-

Mg* is equal MgO/MgO + Fe₂O₃; AI is the alumina index; ASI the alumina saturation index [ASI = molar ratio Al₂O₃ / (CaO + Na₂O + K₂O)], AI is the Apatitic index) = molar (Na₂O + K₂O)/Al₂O₃, AD is the average of 16 samples for major elements concentration from anorogenic Abu Durba porphyries (after El Baily et al., 2022). NES is the average of 70 samples for major elements concentration from anorogenic volcanic rocks, Egypt (after Samiel et al., 2007). A type G is the average of 148 samples for major elements concentration from A-type granites (after Whalen et al., 1987). CC is the averages of the abundance of major elements in continental crust (after Rundick and Fountain, 1995).

Sample No.	S20	S21	S22	S23	S18	S26	S38	S39	S42	S46	Average	S9	S15	S19
------------	-----	-----	-----	-----	-----	-----	-----	-----	-----	-----	---------	----	-----	-----

Li	5.57	10.5	7.39	5.41	4.20	72.9	15.50	37.8	100	7.04	28.83	8.52	5.90	3.22
Be	4.21	2.74	1.96	2.42	3.60	4.76	11.98	11.1	10.6	13.4	5.92	5.41	5.26	4.60
Sc	1.01	1.38	1.16	1.29	1.80	2.08	1.56	1.75	1.86	1.92	1.54	1.60	1.55	1.26
V	1.04	2.00	1.99	1.94	6.54	1.37	2.10	0.41	1.11	0.43	2.06	11.0	0.55	1.68
Cr	1.70	1.87	1.78	2.04	1.47	1.11	2.60	1.99	2.52	1.43	1.90	2.77	1.57	1.38
Co	65.4	54.5	76.0	68.1	39.9	31.6	51.2	76.4	45.9	48.1	56.55	41.0	69.3	37.0
Ni	2.28	3.84	2.09	1.73	1.27	0.79	3.02	1.31	1.92	1.02	2.03	3.56	1.64	1.51
Cu	3.48	5.05	3.06	3.48	2.41	3.74	4.20	3.27	4.00	7.81	3.63	15.3	2.39	6.73
Zn	151	126	44.9	106	122	365	511.0	544	500	488	274.49	250	336	370
Ga	32.0	29.6	27.4	27.8	23.8	42.4	38.6	46.5	46.4	47.9	34.94	25.7	44.9	38.0
Ge	1.65	1.58	1.64	1.57	1.68	2.07	1.77	2.75	2.81	2.75	1.95	1.20	1.51	1.81
Rb	90.1	77.3	94.7	104	374	293	130.6	232	275	229	185.66	137	200	414
Sr	16.2	93.8	26.5	12.1	67.0	16.5	62.5	18.5	20.4	14.3	37.05	61.6	75.7	36.4
Y	70.4	57.0	50.4	50.2	205	145	170.7	216	212	207	130.68	132	159	169
Zr	688	944	665	817	903	1708	1730	1658	1616	1752	1192.06	692	1637	896
Nb	50.2	48.7	42.1	43.0	138	149	135.2	139	152	158	99.68	101	145	143
Cs	0.45	0.81	1.53	1.96	3.46	3.90	1.10	1.61	1.52	1.55	1.82	1.33	0.76	3.17
Ba	28.4	243	63.2	60.9	88.4	38.9	98.6	11.0	13.4	20.0	71.72	111	42.9	68.6
Hf	16.5	18.8	15.0	17.1	34.8	49.6	44.4	48.1	47.6	50.6	32.44	26.8	50.3	35.7
Ta	2.89	3.18	2.68	1.52	12.8	8.54	8.91	6.09	8.54	8.58	6.13	10.1	8.03	6.55
Pb	12.9	14.0	6.71	10.7	105	51.5	36.68	58.3	65.8	52.7	40.12	85.6	22.9	364
Th	9.87	8.82	8.79	8.60	36.1	31.2	27.33	28.3	28.6	30.3	20.83	28.1	30.1	33.4
U	3.80	7.75	2.96	4.35	11.0	13.1	15.99	10.6	11.9	11.5	9.05	8.52	23.2	11.1
Some geochemical ratios														
Zr/Nb	13.70	19.39	15.79	19.00	6.55	11.45	12.79	11.93	10.63	11.12	13.47	6.84	11.30	6.28
Ba/Nb	0.57	4.99	1.50	1.42	0.64	0.26	0.73	0.08	0.09	0.13	1.14	1.10	0.30	0.48
Rb/Nb	31.17	24.30	35.28	68.70	29.10	34.29	14.66	38.13	32.18	26.68	34.20	13.56	24.89	63.21
Nb/Ta	17.36	15.30	15.70	28.36	10.73	17.46	15.18	22.81	17.79	18.37	17.85	9.99	18.05	21.79
Th/Ta	3.41	2.77	3.27	5.67	2.81	3.65	3.07	4.64	3.34	3.53	3.63	2.77	3.75	5.10
Zr/Hf	41.66	50.13	44.50	47.80	25.92	34.44	38.95	34.47	33.93	34.66	39.09	25.83	32.54	25.11
Sr/Y	0.23	1.64	0.53	0.24	0.33	0.11	0.37	0.09	0.10	0.07	0.40	0.47	0.48	0.22
Y/Nb	1.40	1.17	1.20	1.17	1.49	0.97	1.26	1.55	1.39	1.32	1.29	1.30	1.09	1.18

Table 2. Continue

Rock type	Hydrothermal altered aphyric rhyolite					Sheared rhyolite		Calcedony veins		AD	NES	A-type G	CC
	S28	S29	S31	S44	S45	S27	S34	S59	S59R				
Li	3.32	4.86	3.66	4.02	30.20	17.9	7.16	40.5	43.5	-	-	-	-
Be	4.40	3.44	6.07	13.0	12.3	22.0	17.0	2.45	2.44	-	-	-	-

Sc	2.43	2.01	4.72	1.91	1.88	98.2	125	1.79	2.35	-	-	-	-
V	0.60	1.17	0.50	5.58	3.51	1.95	3.08	52.5	53.5	1	17	6	131
Cr	1.08	1.05	1.03	2.18	2.23	3.67	2.99	17.5	17.8	2	12	-	91
Co	18.5	56.3	42.8	20.1	62.2	23.7	20.0	67.1	68.1	-	-	-	-
Ni	0.69	1.14	0.91	3.89	2.82	3.54	0.56	9.84	9.79	-	-	-	-
Cu	4.48	5.44	16.7	4.67	3.99	4.93	3.32	26.4	26.7	-	-	-	-
Zn	59.9	157	120	430	410	168	171	45.1	42.1	-	-	-	-
Ga	44.4	35.8	37.6	43.5	40.3	80.0	34.4	7.15	7.13	-	-	-	-
Ge	2.18	1.43	1.48	1.91	1.85	5.43	4.60	1.01	0.99	-	-	-	-
Rb	202	292	229	102	99	166	256	27.2	26.3	149	165	169	58
Sr	8.75	18.6	19.6	21.9	50.0	56.7	78.5	65.3	65.9	56	85	48	325
Y	185	169	189	197	180	314	303	6.20	5.79	70	58	75	20
Zr	2010	1555	4061	1622	1513	81668	90010	38.2	31.0	834	536	528	123
Nb	128	147	139	177	140	1719	538	2.28	1.75	97	40	37	12
Cs	3.59	1.35	2.33	1.26	1.35	9.81	2.57	1.97	1.97	-	-	-	-
Ba	19.0	63.6	22.7	105	60	17.5	55.8	124	127	298	561	352	390
Hf	53.8	46.0	101	47.3	40.3	1274	1554	1.08	0.86	17	8	4	-
Ta	7.37	4.88	6.89	11.5	10.0	15.8	2.23	0.76	0.66	-	-	-	-
Pb	509	279	43.0	39.3	26.7	389	502	5.70	5.50	15	173	24	13
Th	34.8	25.6	29.5	28.5	29.6	32.6	30.1	0.63	0.49	18	-	23	6
U	16.0	11.0	35.3	11.4	20.5	569	1512	0.98	0.87	4	-	5	1
Some geochemical ratios													
Zr/Nb	15.67	10.56	29.22	9.19	10.80	47.50	167.36	16.74	17.70	-	-	-	-
Ba/Nb	0.15	0.43	0.16	0.59	0.43	0.01	0.10	54.23	72.22	-	-	-	-
Rb/Nb	27.48	59.78	33.17	8.89	9.86	10.52	114.94	35.87	40.01	-	-	-	-
Nb/Ta	17.41	30.19	20.16	15.35	14.00	109.09	241.18	3.01	2.66	-	-	-	-
Th/Ta	4.73	5.24	4.28	2.48	2.96	2.07	13.49	0.83	0.75	-	-	-	-
Zr/Hf	37.33	33.80	40.17	34.29	37.52	64.11	57.92	35.46	36.02	-	-	-	-
Sr/Y	0.05	0.11	0.10	0.11	0.28	0.18	0.26	10.55	11.37	-	-	-	-
Y/Nb	1.44	1.15	1.36	1.12	1.29	0.18	0.56	2.71	3.31	-	-	-	-

AD is the average of 16 samples for major elements concentration from anorogenic Abu Durba porphyries (after [El-Baily et al., 2022](#)). NES is the average of 70 samples for major elements concentration from three localities of anorogenic volcanics NE Sinai, Egypt (after [Samuel et al., 2007](#)). A type G is the average of 148 samples for major elements concentration from A-type granites (after [Whalen et al., 1987](#)). CC is the averages of the abundance of major elements in continental crust (after [Rundick and Fountain, 1995](#))

Table 3. REEs contents (ppm) of Jabal Asfar Thwelil volcanics, Saudi Arabia.

Rock type	Fresh porphyritic rhyolite				Fresh aphyric rhyolite						Average	Hydrothermal altered aphyric rhyolite	
	Sample No.	S20	S21	S22	S23	S18	S26	S38	S39	S42		S46	S9
La	89.7	106	120	97.6	125	67.8	68	62.4	62.1	71.4	87.0	14.0	63.6
Ce	194	220	195	207	118	152	173	162	160	174	175	42.0	49.5
Pr	25.1	28.0	28.9	25.1	33.1	23.1	26.6	24.2	23.8	26.7	26.5	5.28	12.6
Nd	101	109	115	97.3	109	95.0	105	107	103	120	106	22.5	41.2

Sm	18.8	17.8	17.9	16.6	26.4	22.9	22.4	31.8	31.3	35.2	24.1	8.16	14.7
Eu	1.17	1.30	1.20	1.10	0.89	1.05	1.77	1.49	1.48	1.63	1.31	0.42	0.59
Gd	16.0	14.4	14.8	13.9	30.6	22.3	26.2	35.0	34.1	38.2	24.6	12.1	20.4
Tb	2.33	1.99	1.86	1.84	5.53	4.13	4.30	6.12	6.02	6.27	4.04	2.85	4.23
Dy	13.3	11.0	9.95	9.89	33.7	27.2	31.80	37.8	37.2	37.3	24.9	20.3	27.7
Ho	2.57	2.10	1.84	1.84	6.63	5.67	7.11	7.59	7.43	7.41	5.02	4.43	5.66
Er	7.13	5.87	5.08	5.04	18.3	16.8	16.50	21.5	20.6	21.0	13.8	13.3	16.2
Tm	1.05	0.86	0.74	0.72	2.58	2.56	3.84	3.16	2.99	3.11	2.16	2.05	2.41
Yb	6.57	5.46	4.69	4.54	15.2	16.1	17.87	19.2	18.3	19.1	12.7	12.9	14.8
Lu	1.01	0.85	0.72	0.70	2.07	2.30	2.66	2.69	2.57	2.68	1.82	1.80	2.03
Some geochemical ratios													
Eu/Eu*	0.21	0.25	0.23	0.22	0.10	0.14	0.22	0.14	0.14	0.14	0.18	0.13	0.10
(La/Yb)N	9.23	13.19	17.24	14.52	5.55	2.84	2.57	2.20	2.30	2.53	7.22	0.73	2.90
(La/Sm)N	3.01	3.78	4.21	3.70	2.99	1.87	1.91	1.24	1.25	1.28	2.52	1.08	2.74
(Gd/Lu)N	1.95	2.08	2.52	2.45	1.82	1.19	1.21	1.59	1.63	1.75	1.82	0.82	1.23
(La/Lu)N	9.15	12.85	17.06	14.38	6.20	3.02	2.62	2.38	2.48	2.73	7.29	0.80	3.21
∑REEs.	479.76	525.71	517.06	482.85	527.38	458.36	506.95	521.35	511.05	563.93	509.44	162.02	275.56
T1-3	1.01	1.00	0.92	1.00	0.91	1.06	1.05	1.07	1.08	1.04	1.01	1.18	0.89

Table 3. Continue

Rock type	Hydrothermal altered aphyric rhyolite						Sheared rhyolite		Calcedony veins		
	Sample No.	S28	S29	S31	S15	S44	S45	S27	S34	S59	S59R
La		9.19	6.83	20.0	10.6	6.23	20.60	101	103	3.89	3.61
Ce		29.5	16.8	51.5	109	112	190	385	212	9.43	8.70
Pr		4.35	3.01	9.24	4.31	3.65	3.29	70.2	26.7	1.28	1.19
Nd		23.2	16.4	47.8	20.6	20.0	60.1	340	113	6.07	5.69

Sm	14.2	11.5	23.0	10.6	13.7	16.9	110	35.1	1.42	1.35
Eu	0.92	0.81	1.21	0.67	0.91	0.98	4.30	1.64	0.32	0.35
Gd	23.0	20.1	27.0	16.4	24.2	23.0	90.9	39.0	1.31	1.20
Tb	5.22	4.94	5.35	4.03	5.27	5.05	10.9	7.50	0.19	0.18
Dy	34.3	33.4	33.7	29.2	34.2	30.1	56.6	47.9	1.06	0.99
Ho	7.06	6.79	6.85	6.44	7.04	6.06	10.4	9.87	0.20	0.19
Er	19.9	18.7	19.3	19.4	20.1	19.8	27.7	27.8	0.54	0.50
Tm	2.87	2.63	2.87	3.02	3.03	2.95	3.81	4.09	0.077	0.069
Yb	17.4	15.8	16.9	18.6	18.9	16.3	23.2	24.1	0.44	0.40
Lu	2.40	2.18	2.48	2.64	2.67	2.55	3.17	3.54	0.064	0.056
Some geochemical ratios										
Eu/Eu*	0.16	0.16	0.15	0.16	0.15	0.15	0.13	0.14	0.72	0.83
(La/Yb)N	0.36	0.29	0.80	0.39	0.22	0.85	2.96	2.90	5.92	6.03
(La/Sm)N	0.41	0.37	0.55	0.63	0.29	0.77	0.58	1.86	1.73	1.69
(Gd/Lu)N	1.18	1.13	1.33	0.76	1.11	1.10	3.52	1.35	2.50	2.62
(La/Lu)N	0.39	0.32	0.83	0.41	0.24	0.83	3.28	2.99	6.20	6.55
∑REEs.	193.46	159.85	267.17	255.66	271.96	397.58	1237.23	654.87	26.31	24.47
T1-3	1.14	1.09	1.06	1.58	1.73	1.09	1.07	1.04	1.00	1.00

*T1-3 is the third Rare-Earth Elements Tetrad effect calculated (after [Irber, 1999](#))

4.3. Classification and magma type

On the $\text{SiO}_2\text{-Zr/TiO}_2$ diagram of [Winchester and Floyd \(1977\)](#), the analyzed volcanics plot mainly in the comendite/pantellerite field, but porphyritic rhyolite samples straddle the boundary between rhyolite and comendite/pantellerite fields ([Fig. 8a](#)). Using the diagram of Al_2O_3 versus total iron as FeO (after [Macdonald, 1974](#)) as recommended by the IUGS ([Le Maitre et al., 1989](#)), the analyzed lava flows are described mainly as comenditic rhyolite ([Fig. 8b](#)).

The studied JATV are potassic-rich as the $\text{K}_2\text{O}/\text{Na}_2\text{O}$ ratio > 1 and most of the samples have $\text{A}/\text{CNK} < 1.15$ ([Table 1](#)), which indicate their alkaline nature ([Liégeois et al. 1998](#)). By plotting the Al saturation index (AI) against SiO_2 most of JATV samples fall within the range of metaluminous alkaline to peralkaline domains ([Fig. 8c](#)) and they are following the decreasing trend of Pan-African peralkaline granites suggested by [Hadj-Kaddour et al. \(1998\)](#). On the alkalinity index- Fe number (F^*) diagram ([Frost and Frost, 2008](#)), these alkaline rhyolites are mainly metaluminous to slightly peralkaline ([Fig. 8d](#)). There are two samples are weakly peraluminous (i.e. corundum-normative; $\text{A}/\text{CNK} = 1.01\text{--}1.07$) and 2 other samples are peralkaline (i.e. acmite-normative; $\text{NK}/\text{A} > 1$). The JATV samples are classified as ferroan and plot in A-type field ([Fig. 8e](#)) as shown on the $\text{FeO}/(\text{FeO} + \text{MgO}) - \text{SiO}_2$ diagram of [Frost et al. \(2001\)](#). The alkaline affinity of JATV is demonstrated on the discrimination diagram of [Sylvester \(1989\)](#), as most of the sample plots fall in the alkaline granite field ([Fig. 8f](#)), except highly

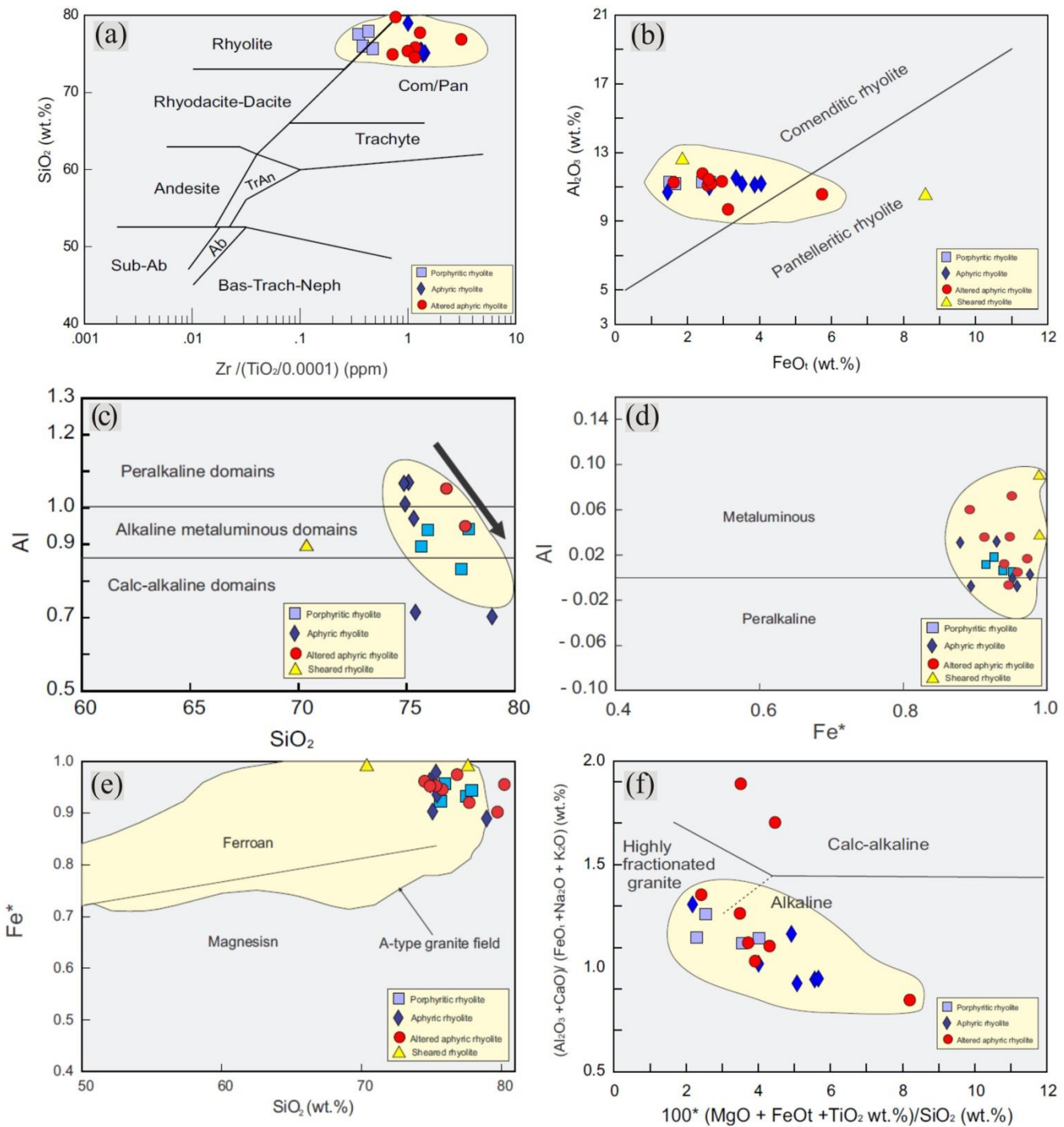


Fig. 8. a) SiO_2 -Zr/TiO₂ diagram (Winchester and Floyd, 1977); b) Al_2O_3 – FeO_t diagram (Macdonald, 1974); c) Agpaitic index (AI) vs. SiO_2 diagram, the line with AI= 0.87 after Liégeois and Black (1987) separates alkaline and calc-alkaline granite series; black solid arrow represents the evolution of Pan-African peralkaline granites from Algeria (Hadj-Kaddour et al., 1998); d) AI-Fe* (Frost and Frost, 2008); e) Fe* versus SiO_2 (Frost et al., 2001). Note: AI (Agpaitic index) = molar $(\text{Na}_2\text{O} + \text{K}_2\text{O}) / \text{Al}_2\text{O}_3$, Fe*(Fe index) = $(\text{FeO}_t / \text{FeO}_t + \text{MgO})$; f) $\text{Al}_2\text{O}_3 + \text{CaO} / \text{FeO}_t + \text{K}_2\text{O} + \text{Na}_2\text{O}$ versus $100 * (\text{MgO} + \text{FeO}_t + \text{TiO}_2) / \text{SiO}_2$ discrimination diagram (Sylvester, 1989).

altered two samples plot in the calc-alkaline granite field. The studied JATV possess the major element characteristics of A-type granites suggested by Whalen et al. (1987), for example: $\text{K}_2\text{O}/\text{MgO} > 16$, $(\text{Na}_2\text{O} + \text{K}_2\text{O})/\text{CaO} > 10$ and agpaitic index (AI) > 0.85 (Table 1). Furthermore, the JATV trace elements contents carry the characteristics of A-type granites, which are high in Zr (> 250 ppm), Nb (> 20 ppm), Zn (> 100 ppm), and Ce

(>100 ppm) (Collins et al. 1982; Eby 1990; Bonin 2007; Frost and Frost 2011; Bonin et al. 2020). Whalen et al. (1987) suggested plots of Ga/Al versus certain major and trace elements to distinguish between A-type granites and other granites (M-, I- and S-type granites). On the Ga/Al versus FeO*/MgO diagram, all the volcanic samples are plotted in the A-type field (Fig. 9a).

4.4. Spider diagrams and REE patterns

Primitive mantle-normalized spider diagrams of the studied rocks (using the normalization values of Sun and McDonough, 1989), are shown in figure (9b). The lava flows show nearly similar patterns and characterized by enrichment in large-ion lithophile elements (LILE) relative to the high field-strength elements (HFSE) and have negative anomalies in Sr, Ba, P and Ti (Fig. 9b). The sheared rhyolite samples show enrichment in Nb, Zr and Hf than other volcanic samples (Fig. 9b). The spider diagrams of the chalcedony are completely different from the lava flows (Fig. 9b), as they show depletion in all trace elements than the volcanic samples. The prominent negative Sr, B, P and Ti anomalies (Fig. 9b) imply feldspars, apatite, and Fe-Ti oxide fractionation, respectively. The low Ba and Sr values (Fig. 9b) reflect extensive feldspar fractionation.

Concentrations of REEs. are given in table (3) and the chondrite-normalized REE patterns (using the chondrite values of Evensen et al., 1978) are presented in figure (9c). The normalized REEs. patterns of the analyzed lava flows show wide variations due presence of different accessory minerals and may be the affect of different styles of alterations. This depends, most probably, on the nature of the crystallizing accessory mineral phases, where monazite will deplete the melt in the Light Rare-Earth Elements (LREEs.), zircon in the Heavy Rare-Earth Elements (HREEs.) and apatite in the Middle Light Rare-Earth Elements (MREEs.), (Rollinson, 1994). The sheared rhyolite contains the highest content of the REE (655-1237 ppm), while the chalcedony samples contain the lowest content (24-26 ppm; Table 3).

The porphyritic rhyolite shows LREEs. enrichment relative to HREEs. [(La/Lu)_N = 9.15-17.06; Table 3] with obvious negative Eu anomaly [(Eu/Eu*)_N = 0.21-0.25]. The fresh aphyric rhyolite samples have high content of REE (458-564 ppm) than the altered samples (160-398 ppm). On the other hand, the fresh aphyric rhyolite samples are slightly enriched in light REE than heavy REE [(La/Lu)_N = 2.38-6.20], but the altered samples are rich in HREEs. than LREEs. [(La/Lu)_N = 0.24-0.83; except sample No. S19]. All samples of aphyric rhyolites show negative Eu anomaly [(Eu/Eu*)_N = 0.10-0.22]. Few altered aphyric rhyolite samples show positive Ce-anomaly, which is not present in the other samples. Generally, the alteration of the rock is the possible explanation.

Negative Eu anomalies in the analyzed lava flows might indicate early fractionation of plagioclase or the partial melting of a source rock in which feldspar is retained in the residue (Ragland 1989; Wilson 1989; Rollinson, 1994). The sea gull REE pattern (Fig. 9c), due to deep negative Eu anomaly, is a characteristic feature of hot-dry-reduced magmas with relatively low oxygen fugacity, that were formed in the terrains of mantle upwelling (i.e. hotspots and continental rifts; Christiansen 2005; Bachmann and Bergantz, 2008; Christiansen and McCurry, 2008; Deering et al., 2010; Frost et al., 2016; Kuibida et al., 2020; Szemerédi et al., 2020; El-Bialy et al., 2022). In all analyzed volcanics there is interrelation between the Eu anomaly and the Ba and Sr concentrations that reveals that the strong negative Eu anomalies are mostly associated with the low Ba and Sr concentrations indicating extreme alkali feldspar fractionation. The REEs patterns of the JATV is slightly enriched in HREEs. compared to those of Gabal Abu Durba granite and rhyolites porphyry (El-Baily et al., 2022) and Katherina Volcanics (KV) (Samuel et al., 2007; El-Bialy and Hassen, 2012; and Azer et al., 2014) (Fig. 9c).

V. Discussion

The last phase of evolution of the Arabian Shield included vast intrusion of alkaline plutonic rocks and their volcanic equivalents. The evolution of JATV is discussed here in light of the current data and the larger context of alkaline magmatism in the Arabian Shield.

5.1. Geotectonic affinity

It is now widely accepted that during the late stage of evolution of the Arabian Shield, the subduction-related calc-alkaline magmatism was replaced by post-tectonic alkaline magmatism (Harris, 1982; Bendor, 1985;

Abdallah et al., 2020; Abuamarah et al., 2021; Gahlan et al., 2021, 2022). The overall chemical characteristics of the studied volcanics are consistent with a within-plate tectonic setting. They show remarkable depletion in CaO, MgO, Sr and marked enrichment in Nb, Y, Ta, Hf and Th (Tables 1, 2; Fig. 9b). These geochemical features are typically characteristic of within-plate magmatism in the Arabian-Nubian Shield (Azer et al., 2014; Samuel et al., 2007; Khalil et al., 2018). In addition, Schandl and Gorton (2002) used some immobile High-Field Strength Elements (Ta, Yb, Th), to discriminate felsic to intermediate volcanic rocks ($\text{SiO}_2 = 54\text{--}77$ wt.%) from oceanic arcs, active continental margins, and within-plate volcanic zones. As shown on the Yb–Th/Ta diagram, the investigated JATV are interpreted as within-plate volcanics (Fig. 9d). Agrawal, (1995) employed the major oxides to calculate r_1 and r_2 (Table 1) multivariate discrimination diagram to distinguish between Orogenic, late-Orogenic, Post-Orogenic and Anorogenic tectonic environments for the granitic magma. The studied JATV falls within Anorogenic tectonic field (Fig. 9e).

5.2. Magma melting temperature

By using Al-Ti thermometer method that calibrated by Jung and Pfänder (2007) (Table 1), the melting temperatures of JATV rocks fall within the range between a minimum of 804°C and a maximum of 915°C, with an average temperature 866 °C. This value is slightly higher than the averages temperature estimated by El-Bailly and Hassen (2012) for late Ediacaran, A-type alkaline rhyolites of Gabal Ma'ain, Sinai (i.e., 848 °C) and El-Bailly et al. (2022) for late Ediacaran granite-rhyolite porphyries of Gabal Abu Durba, Sinai (i.e., 848 °C), Sinai, Egypt, in the ANS.

5.3. Magma sources

A-type magmas are broadly accepted to be generated in a variety of late to post-orogenic and anorogenic settings (Collins et al. 2019; Barbarin 1999; Bonin et al. 2020). These models are: a) A-type magmas are results of fractionation of mantle-derived mafic magmas, with or without participation of crustal rock (Stern and Gottfried, 1986; Eby 1990, 1992; Bonin, 2007; El-Bialy and Hassen 2012; Grebennikov 2014; Salih and Abdel Rahman 2021); b) partial melting of different pre-existing crustal rocks (Dall'Agnol et al. 1999; Martin 2006; Farahat et al., 2007; Salih et al. 2020); c) recently the mixing of mantle-derived magmas and crustal materials through a successive fractional crystallization process succeeded getting to be admitted for generating A-type magma (Kemp et al. 2005; Whalen et al. 2006; Farahat et al., 2011, Farahat and Azer, 2011; El-Baily et al., 2022).

5.3.1. Role of crustal material

The geochemical data of the studied volcanics can furnish, to some extent, criteria for their petrogenesis. The absence of intermediate and mafic lithologies associating the JATV argues against an origin from fractional crystallization of mantle-derived mafic magma. The studied volcanics comprise rhyolitic ignimbrite and many petrologists have suggested the importance of crustal melting in the generation of ignimbrites (Coulon et al., 1978; Gill, 1981; Wilson, 1994; Chalot-Prat, 1995). The ratios of the highly incompatible trace elements are characteristic of the source region from which the magma was extracted. The analyzed samples of JATV show a remarkably low content of Ni (avg.= 1.85 ppm), Cr (avg.= 1.93 ppm) along with Mg^* values range between ($\text{Mg}^* = 4.22\text{--}19.74$) (Table 2). All of these geochemical features argue against the mantle origin of the studied volcanic rocks, where the primitive magmas extracted from the mantle should have high $\text{Mg}^\#$ (68–75), Ni (> 250 ppm) and Cr (> 1000 ppm) contents (Perfit et al., 1980). The relative enrichment of Rb, Th, Pb, and total REEs. (Table 3) beside depletion in Sr, P, Ti (Fig. 9b) and Eu negative anomaly (Fig. 9c), suggest incorporation of a crustal component (e.g. Green et al., 2000). Moreover, the Zr/Nb, Ba/Nb and Rb/Nb geochemical ratios of the studied volcanics have averages of 22.35, 31.12 and 1.57,

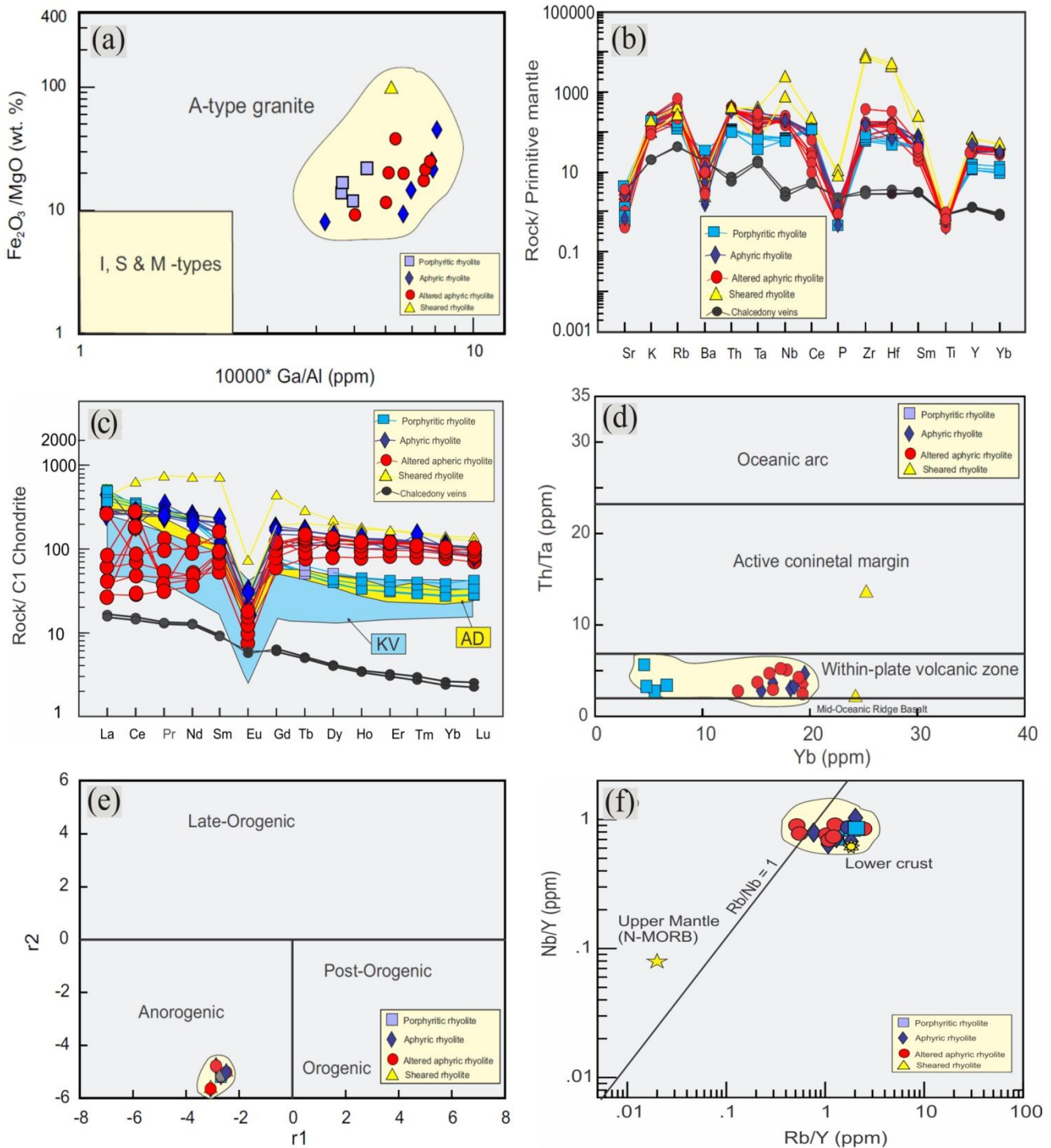


Fig. 9. a) $FeO^*/MgO - 100000 * Ga/Al$ classification diagram (Whalen et al., 1987); b) Primitive mantle-normalized spider diagrams of JATV (using the normalization values of Sun and McDonough, 1989), c) Chondrite REEs. plots the Chondrite-normalization values are from Evensen et al. (1978). Note: yellow field for Gabal Abu Durba granite and rhyolites porphyries from El-Baily et al. (2022), ice blue field of Katherina Volcanics (KV) based on data from Samuel et al. (2007) El-Bialy and Hassen (2012) and Azer et al. (2014); d) Yb vs. Th/Ta (Schandl and Gorton, 2002) tectonic discrimination diagram illustrating tectonic setting of the JATV; e) r1-r2 multivariate discriminant diagram (Agrawal, 1995) for the studied JATV; f) Nb/Y- Rb/Y diagram (modified after Chazot and Bertrand, 1995). Note: the composition of the lower crust is from Rudnick and Gao (2003) and that of the upper mantle (N-MORB) is from Sun and McDonough (1989). These averages lie within or near the ranges of values currently in use for the continental crust (Weaver, 1999; Wedepohl, 1994). Furthermore, the mantle source magmas have Y/Nb ratios less than 1.2, while most of analyzed samples have $Y/Nb \geq 1.2$ (Table 2), which characterizes rocks of crustal origin (Eby

1990; 1992), which argue against mantle source for JATV. To determine the source of the studied JATV, the Nb/Y-Rb/Y diagram used to compare their composition with lower crust and upper mantle composition. The JATV samples just plots around to the lower crust composition (Fig. 9f). Furthermore, fresh samples of JATV have high concentrations of Pb (6.71–56.80 ppm; 41.43 ppm on average; Table 2) relative to mantle-derived melts (Pb: ~ 0.38 ppm; Zartman and Doe 1981), this is inconsistent with strictly mantle-derived origin.

5.3.2. Role of mantle material

The Zr/Hf ratios (38.64 on average) of JATV (Table 2) exceed both the continental crust values (33 ppm; Rudnick and Fountain, 1995) and the chondrite value (34.3 ppm; Weyer et al. 2003) but fall within the range of depleted mantle values (35.7–45.53; Kamber and Collerson 2000). Similarly, the Nb/Ta ratios (10.78–28.29; 17.86 on average) of the studied JATV (Table 2) mostly exceed the Nb/Ta values of continental crust (~ 11–12; Rudnick and Gao. 2003; Huang et al., 2011). The Th/Ta ratio was considered by Shellnutt et al. (2009) as an indicator of crust–magma interaction. This ratio close to 2, lesser than the upper continental crust and lower continental crust (i.e., Th/Ta = 6.9 and 7.9 respectively). The Th/Ta of JATV ratio has an average of 3.62 (Table 2), which is consistent with mantle derivation and insignificant crustal contamination.

Furthermore, the relative enrichment in HFSE (Zr, Hf, Nb, Ta, Y; Table 2), absence of negative Nb anomalies (Fig. 9b), and enrichment in HREE (i.e, between 30–120 times chondrite) (Fig. 9c) support the mantle derivation hypotheses of JATV A-type magma and argue against crustal contamination and or assimilation role. The geochemical data of the studied volcanics show evidence for rifting during the emplacement of the JATV. On SiO₂ vs. Al₂O₃ diagram of Maniar and Piccoli (1989), most analyzed volcanics plot in the rift-related granite field (Fig. 10a). The emplacement of the studied volcanics has most probably occurred along Pan-African fractures that have been re-activated by relaxation after the termination of the Pan-African orogeny. All the obtained data for the JATV suggest that these volcanics might have been formed by fractionation of melts derived from continental source rocks.

The very low Ba/Sr and Sr/Y ratios (0.05–314 and 0.07– 1.64, respectively; Table 2), the presence of strong negative Eu-anomalies and the HREEs are not depleted as the Yb and Lu are 80–150 times chondrite, indicating that JATV formed at relatively low oxygen fugacity (i.e., hot-dry- reduced magma; Bachmann and Bergantz, 2008; El- Bialy and Hassen, 2012; Frost et al., 2016; Kuibida et al., 2020; Szemerédi et al., 2020). The hot-dry magma with its characteristics sea-gull REEs pattern due to the steep negative Eu anomaly and enriched HREEs (Fig. 9c), suggest that the JATV magma source was garnet-free (Laurent et al., 2014; Wilson, 1989). The garnet-free magma source implies a shallow mantle source rather than deep one, where the stability of spinel is higher than garnet in shallower levels (Ragland 1989; Rapp and Watson 1995). In addition, the remarkable enrichment of incompatible trace elements (i.e. Zr, Nb, Zn, Ga, Y, Ce; Fig. 9b) suggests an enriched mantle source for JATV. The enriched mantle source is comparable with ocean island basalts (Wittke and Mack, 1993; Hofmann, 1997), which is not in accordance with both the depleted lithospheric mantle source of normal mid-oceanic ridge basalt and island arc basalt, suggesting that the asthenosphere was favorable mantle source for JATV.

Overall, depending on their trace element contents and some specific geochemical ratios, confirms beyond a reasonable doubt that, the JATV were derived from asthenospheric mantle comprising a crustal component, which either recycled component from pre-collision event or a recycled component in the source.

5.4. Fractional crystallization

The overall chemical characteristics of the JATV suggest the role of fractional crystallization process during the generation of their parental magma. The absence of xenoliths in the studied volcanics indicates that crustal contamination has no role in the evolution of magma that producing these rocks. K-feldspar is the main fractionating phase during the evolution of these volcanics as evidenced by the moderate correlation with fairly steep slope in the logarithmic plot of Ba against Sr (Fig. 10b). The fractionation of feldspars is supported by the plot of 1/Sr vs. Rb/Sr (Fig. 10c). The pronounced negative Eu anomalies (Fig. 9c) provide evidence for the fractional crystallization of feldspars from parental magmas at depth (Hanson, 1978; McKay, 1989). Furthermore, as the LILE/HFSE ratios (Th/Nb) should not be significantly affected by fractional crystallization,

these ratios were plotted against an incompatible trace element (Zr) (Fig. 10d) whose abundance increases as fractionation increases. On this diagram, the magmatic evolutions controlled by simple fractional crystallization in closed systems produce a horizontal trend with increasing crystal fractionation. The studied rhyolite lavas define a horizontal trend characterized by nearly constant Th/Nb elemental ratios (Fig. 10d), proving that the fractional crystallization was the main process during magmatic differentiation. Moreover, the relative depletion of the JATV in Sr, Ba, P, and Ti (Fig. 9b) is most likely the result of crystal fractionation. Sr and Ba are presumably related to the fractionation of feldspars, while P and Ti are controlled by the fractionation of apatite and Fe-Ti oxide, respectively (Green, 1980; Bevins et al., 1995).

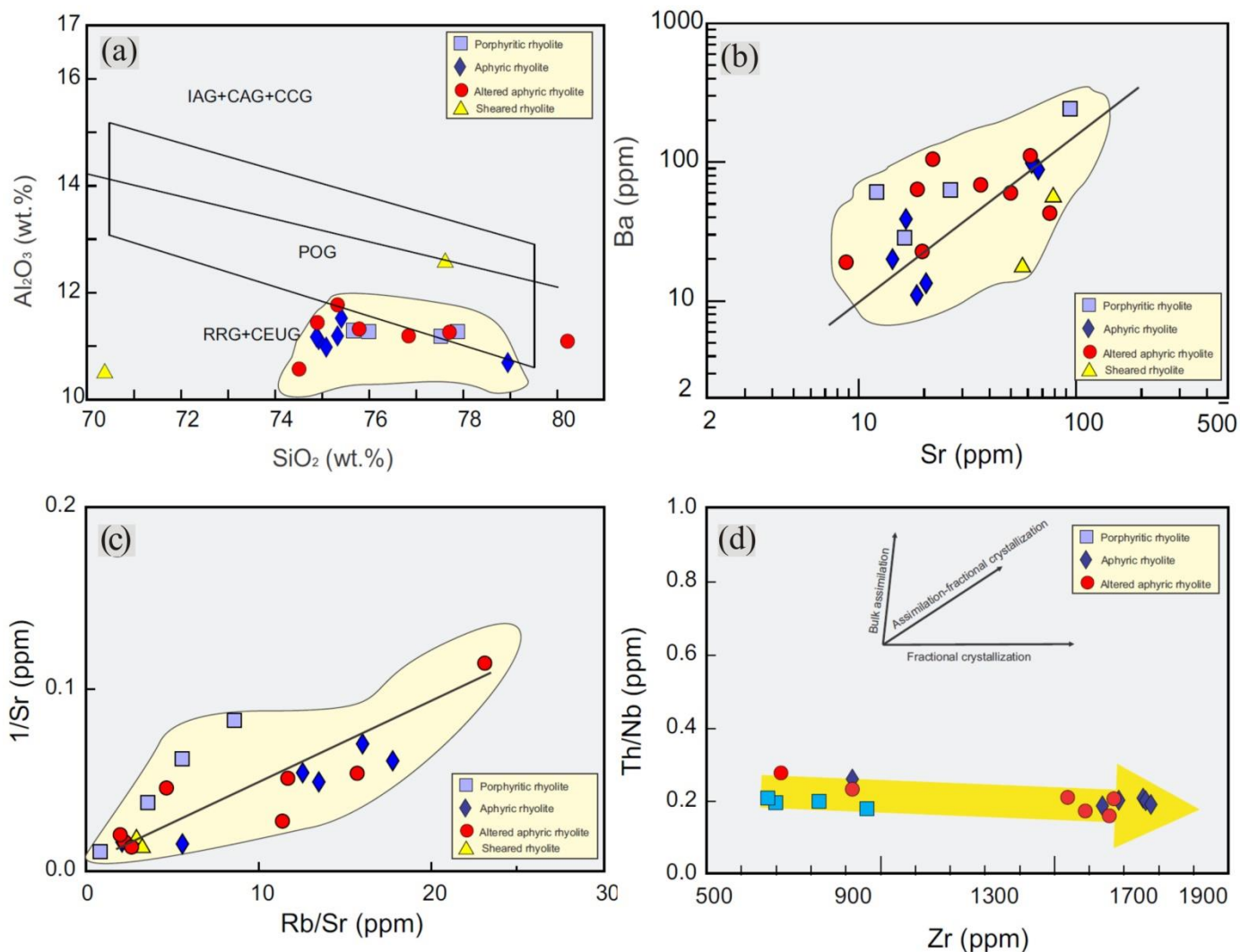


Fig. 10. a) SiO_2 vs. Al_2O_3 diagram of Maniar and Piccoli (1989). Note: IAG, island arc granitoids; CAG, continental arc granitoids; CCG, continental collision granitoids; POG (post orogenic granitoids), RRG (rift-related granitoids), CEUG (continental epeirogenic uplift granitoids); b) Ba vs. Sr binary diagram; c) $1/Sr$ vs. Rb/Sr binary diagram; d) Fractional crystallization vector binary Th/Nb-Zr diagram, fractional crystallization, assimilation-fractional crystallization, and bulk assimilation trends are from Nicolae and Saccani (2003).

6. Reginal geodynamic implications

As stated before, JATV is considered as one of the essential recent volcanic units in the Arabian Shield with an age (~ 572 Ma; Hadley and Schmidt, 1980). They intrude tonalite-granodiorite suite (~ 738 Ma; Quick and Doebrich, 1987) and in turn intruded by alkaline granites and gneophyres (575-580 Ma; Stuckless et al., 1984), so the JATV mark the final stage in the Precambrian history of the ANS. At this stage magmatism shifted from calc-alkaline to alkaline and the tectonic regime and the emplacement of magmas changed from collision

through post-collision, to within-plate extension. Recently, the widely distributed calc-alkaline and alkaline coeval suites, which constitute ~ 80 of the total basement complexes in the northern ANS (Stern and Hedge, 1985) and the transition from calc-alkaline (~630-590 Ma) to alkaline (~610-580 Ma) magmatism during evolution of ANS explained in terms of lithospheric delamination (Farahat et al., 2007, 2011; Avigad and Gvirtzman, 2009). The lithospheric delamination involves lithospheric removal subsequent to crustal and mantle thickening and subduction break-off during the collisional stage. Such lithospheric removal, results in upwelling the hot lighter asthenosphere and crustal uplifting, up to ~3 km in the northern ANS (Avigad and Gvirtzman, 2009). The continental collision (~670-630 Ma) leads to extensive crustal thickening (Stern 1994, 2002; Abdelsalam & Stern 1996; Stoesser & Frost 2006; Stern 2008; Avigad & Gvirtzman 2009; Fig. 11a), while the extensional collapse (600-550Ma), which was controlled by lithospheric delamination and slab breakoff, leads to thinning of lithosphere (Davies & von Blackenburg, 1995; Farahat et al. 2007, 2011; Avigad & Gvirtzman, 2009; Eyal et al. 2010; Farahat and Azed, 2011).

During late collisional stage (630-610 Ma) between the East and West Gondwana (Abdelsalam et al. 2002), at the beginning of the slab breakoff (Fig. 11a), a slab window opened (Fig. 11b). This slab window enhancing the heat flux that provided by the upwelling asthenosphere, causing lithospheric mantle melting (Bonin, 2007). This melt produced underplate the lower crust to promote their partial melting processes and generate coeval late-collisional calc-alkaline magmatism (Farahat et al., 2011) in the northern ANS (Fig. 11c). The next late collisional to early post-collisional stage (610-590 Ma) commenced ~20 m.y. later on, the rapid uplift of the crust due to the slab detachment caused decompression melting in the mantle lithosphere (Fig. 11c). The generated mafic mantle-derived melt causing widespread magmatism and the heat flux provided by the upwelling asthenosphere leads to partial melting of lower crust, which producing coeval calc-alkaline/alkaline magmas (Fig. 11c).

During the late post-collisional crustal extensional stage (590-550 Ma), the effects of lithospheric delamination, and thus of the asthenospheric uprise, are likely diminishes (Farhat and Azer, 2011). The upper mantle-derived melts produced in turn as a result of decompressional melting due to erosional uplifting and consequently this alkaline/peralkaline melt intraplate the middle crustal level. This intraplate process is facilitated by the abundance of strike-slip faults and shear zones (e.g. Shammar shear). At this stage this melt either form A-types plutonic complexes or continue to arrive as shallow crustal magma chambers to form JATV (Fig. 11d).

7. Metasomatic alteration of JATV

Some of HAAR and the sheared rhyolite samples have extremely high concentrations of Zr and U (Table 2). Uranium mineralization is found filling cavities and as surface encrustations on some crystalline rocks of the ANS (e.g. Abd El-Naby, 2008; Abu Elatta et al, 2013; Dawood et al., 2014; Gaafar, et al., 2014; Shalaby et al., 2015; Ibrahim et al., 2017; Dawood and Abd Naby, 2022). Uranium is sometimes concentrated in medium alkalinity rocks and alteration processes (i.e. albitization, carbonatization, and ferrugination) may affect the U content in these rocks (i.e. Kouske et al., 2012). U-mineralization is also found in felsic to intermediate volcanic rocks, volcanoclastic rocks, and ring dykes (Saleh et al., 2021). Increase U and Zr contents in metasomatized alkaline volcanics in Germany is reported by Ulrych et al., (1990b) and peralkaline volcanics in ANS by Abu Elatta et al, (2013). The recent studies did not record any primary uranium minerals and they attributed the source of uranium in the fluids to high-T alteration processes for U-rich accessory phases, such as zircon and monazite, in addition to labile uranium which is occurred among rock grains (Dawood and Abd Naby, 2022).

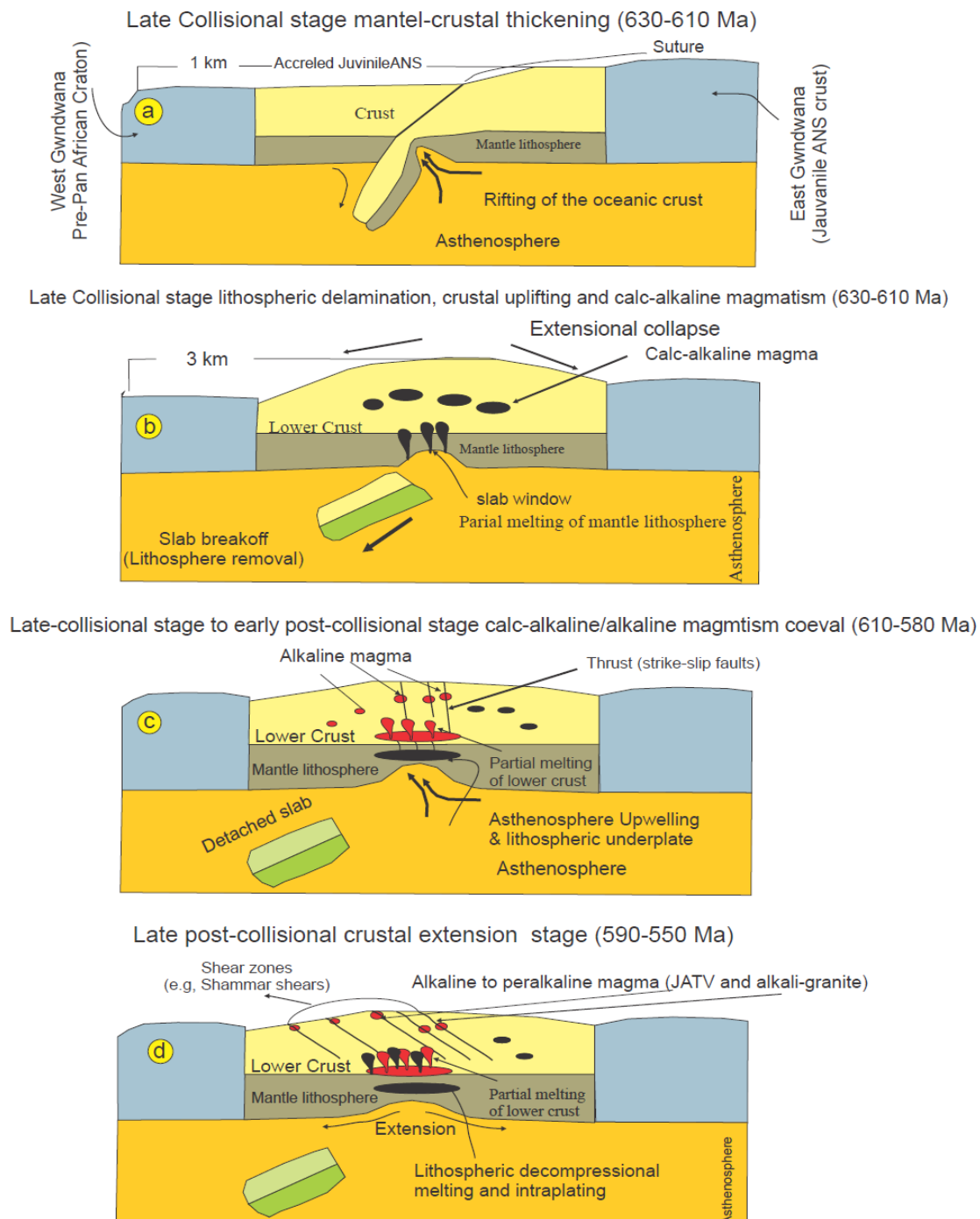


Fig. 11: Sketch showing the tectono-magmatic evolution of late Ediacaran A-type JATFV (modified after Davies and von Blanckenburg 1995; Eyal et al. 2010; Farahat et al., 2007, 2011; Farahat and Azer 2011; Moghazi et al. 2011; Eliwa et al. 2014; Elwan 2019; Elwan et al., 2019), a) Late collision stage between East and West of Gondwana (630–610 Ma), which characterized by mantle/crust thickening and beginning of oceanic crust rifting; b) Beginning of the extensional collapse at ~ 600 Ma and slab breakoff as a consequence of crustal thickening. Due to slab breakoff a slab window opened, which enhance heat flux provided by the upwelling asthenosphere, causing melting, which produced late-collisional calc-alkaline magmatism; c) Slab detaches and sink away and the detached slab or lithospheric removal allows asthenosphere to rise or asthenosphere upwelling causing melting, which followed by underplating of this melt and formation of calc-alkaline /alkaline magmatism; d) Rapid lithospheric uplift and intraplating caused melting to produce alkaline/peralkaline magmatism in ANS, which facilitated by strike-slip faults and shear-zones and some Asthenosphere upwelling (Farahat and Azer 2011). The alteration profile of the studied JATV shows the illite formation trend (Fig. 12a). According to the mass-balance isocon diagram of Grant (1986), the HAAR are enriched in Zr about 20 time more than the unaltered rhyolite with an average (Zr = 22816.13 ppm or 2.28

wt.%). U gains 33 times more than fresh rhyolite with an average of 273.27ppm, while Hf gains 12 times, Nb gain 3 times more than fresh rhyolite. HAAR are slightly enriched in Y, Th, Sr, Rb, Ga and they are depleted in Na₂O, Zn, MnO and LREEs (Figs. 9b, c & 12b). The HAAR samples enriched K₂O is depleted in Na₂O (Table 1). Sheared rhyolite strongly enriched in Zr that it gains 64 times more than fresh rhyolite with an average (Zr = 85839.04 ppm or 8.58 wt.%). U gains 104 times more than fresh rhyolite with an average (U = 1040.46 ppm or 0.10 wt.%). Hf gains 38 time, Nb gains 9 times, Pb gain 18 times and P₂O₅ gain 8 times more than fresh rhyolite. Sheared rhyolites are slightly enriched in Y, Fe₂O₃, Ga, Sr, Th and REEs (Figs. 9b, c & 12c) and they are depleted in Na₂O, MgO and Zn. Most of HAAR have Rare-Earth tetrad effect with values of third tetrad (T1-3) > 1 (i.e., prominent tetrad effect (Irber, 1999; Table 3). The REEs tetrad effect is most visible in late magmatic differentiates with strong hydrothermal interaction or deuteric alteration (Jahn et al., 2001). Three samples of hydrothermally altered rhyolite show positive Ce-anomalies, while four samples show negative Ce-anomaly (Fig. 9c). These three samples are strongly illitized, illitization destruct plagioclase and form illite-hematite and secondary U-bearing minerals assemblage. Argillic alteration is representative of supergene environments where low temperature groundwater becomes acidic. This process includes liberation of free Ca²⁺ and CO₃⁻ ions. Möller and Bau (1993) argued that the development of a positive Ce-anomaly in aerobic alkaline fluids may be explained by the stabilization of penta-carbonato-Ce^{IV}-complexes that hold Ce⁴⁺ in fluid, leading to enhanced abundances of Ce in comparison with its trivalent REEs neighbors. In those conditions of alkaline fluids and at low temperature the REEs, especially Eu and Y tend to make complexes with sulfate and carbonate more than chloride or fluoride. On the other hand, the negative Ce-anomaly suggests the circulation of external oxidizing fluids, which were most probably of meteoric origin (Hecht et al., 1999). The high concentrations U in HAAR and sheared rhyolite attributed to the illitization of plagioclase and formation of secondary U-bearing minerals. The destruction of plagioclase is commonly accompanied by liberation of free Ca²⁺ and CO₃⁻ ions and U in 6⁺ oxidation state tends to make complexes, these complexes are uranyl carbonate, hydroxide, silicate, phosphates, sulfates and fluorides. Boctor and Yoder (1986) and Dawood and Abd Naby (2022) related the crystallization of the U, Zr-bearing minerals in alkaline volcanics at supergene or low-temperature post-magmatic hydrothermal phase, where the precipitation of U- mineralization occurred when the residual late hydrothermal fluids cool to the temperature of meteoric water and that facilitated by the presence of faults or brecciated shear zones, characterized by strong alteration.

The slightly increase in HREEs. of HAAR and overall REEs. of sheared rhyolite (Fig. 9c) could be attributed to the post-magmatic low temperature fluid enriched in incompatible elements including Zr and REEs. The shear zones served as a feeding channel for incompatible elements-rich hydrothermal fluids. These high U and Zr concentrations in both hydrothermally altered aphyric and shared rhyolites are promising, and the area could be containing an economic deposit of U and Zr.

VI. Summary

- At the late stage of the Arabian Shield evolution, Jabal Asfar Thwelil volcanics (JATV) were erupted during a non-orogenic period. Petrographically, they are exclusively subaerial and unmetamorphosed. They are represented by rhyolitic lava flows, pyroclastics and ignimbrites. The lava flows include porphyritic and aphyric rhyolites. The rhyolites are either alkaline or peralkaline (comendites) carrying acmite normative.
- The REE patterns depict pronounced negative Eu anomalies. The overall chemical characteristics of the studied volcanics are consistent with A-type metaluminous to peralkaline magmatic source, which were emplaced in anorogenic rift-related tectonic setting.
- There is a package of geochemical clues support derivation of JATV from mantle, for instance, their relative enrichment in HFS, lack of negative Nb anomalies, their enrichment in HREE, and their characteristic values of the Zr/Hf, Nb/Ta, Th/Ta Y/Nb Yb/Ta geochemical ratios. Nevertheless, the remarkably low content of Ni, Cr along with Mg* values, the mild enrichment in Th, Rb, Pb and total REE and depletion in Sr, P, Ti and the characteristic values of geochemical ratios such as and Rb/Nb, Y/Nb may imply restricted incorporation of a crustal component. The suggested crustal source of these volcanics is

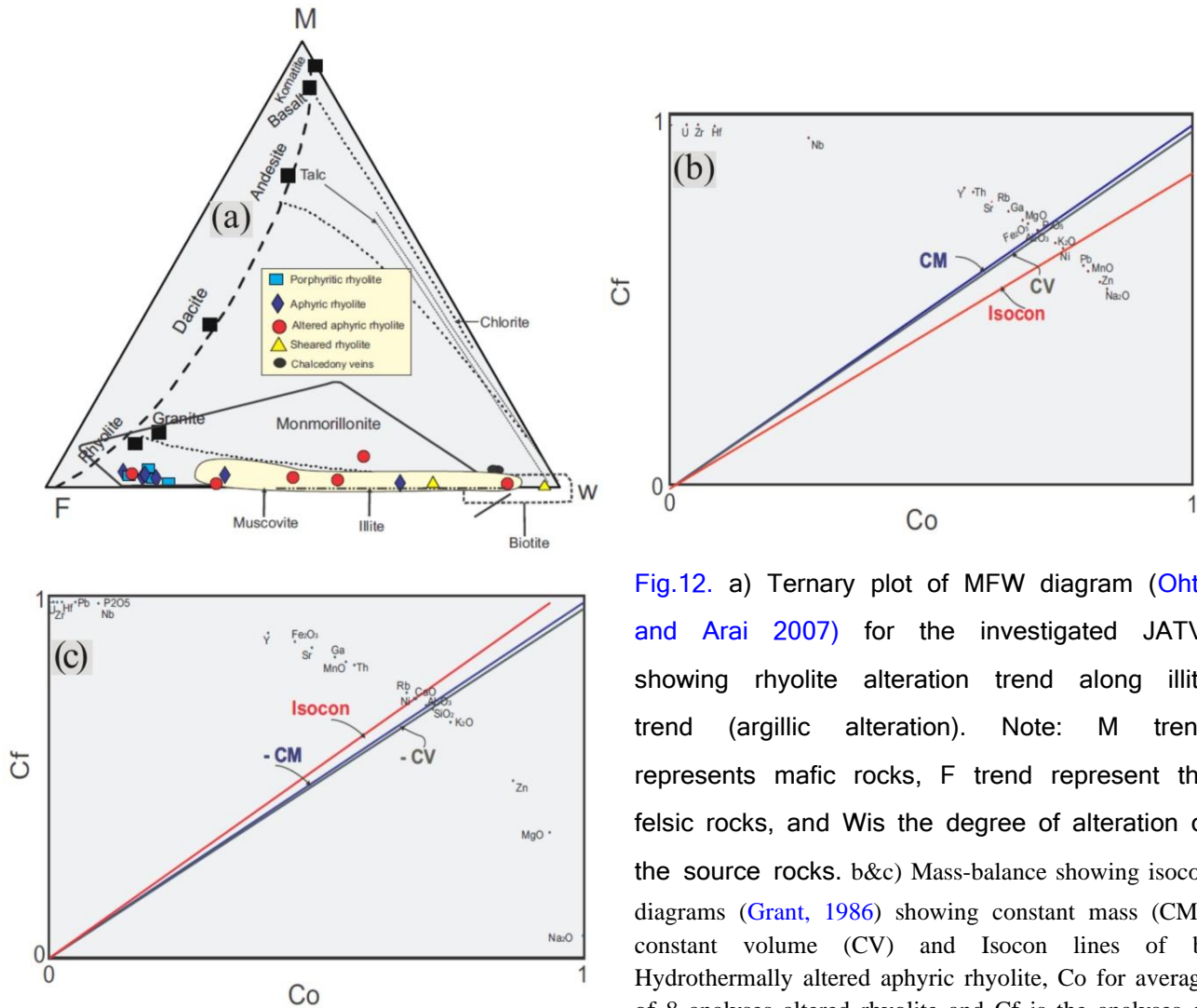


Fig.12. a) Ternary plot of MFW diagram (Ohta and Arai 2007) for the investigated JATV, showing rhyolite alteration trend along illite trend (argillic alteration). Note: M trend represents mafic rocks, F trend represent the felsic rocks, and Wis the degree of alteration of the source rocks. b&c) Mass-balance showing isocon diagrams (Grant, 1986) showing constant mass (CM), constant volume (CV) and Isocon lines of b) Hydrothermally altered aphyric rhyolite, Co for average of 8 analyses altered rhvolite and Cf is the analyses of

plagioclase-rich and garnet-free residue. In other words, the JATV were derived from asthenospheric mantle comprising a crustal component, which either recycled component from pre-collision event or a recycled component in the source.

- There is a package of geochemical clues support derivation of JATV from mantle, for instance, their relative enrichment in HFS, lack of negative Nb anomalies, their enrichment in HREE, and their characteristic values of the Zr/Hf, Nb/Ta, Th/Ta Y/Nb Yb/Ta geochemical ratios. Nevertheless, the remarkably low content of Ni, Cr along with Mg* values, the mild enrichment in Th, Rb, Pb and total REE and depletion in Sr, P, Ti and the characteristic values of geochemical ratios such as and Rb/Nb, Y/Nb may imply restricted incorporation of a crustal component. The suggested crustal source of these volcanics is plagioclase-rich and garnet-free residue. In other words, the JATV were derived from asthenospheric mantle comprising a crustal component, which either recycled component from pre-collision event or a recycled component in the source.
- Geochemistry data of the JATV suggest that the parent magma has undergone some degree of magmatic differentiation. Alkali feldspars were the main fractionating phases; fractionation of apatite and Fe-Ti oxides played a minor role.
- The obtained data demonstrate that most of the volcanic samples are suffered from different degree of metasomatic alterations including, silicification, sericitization and illitization specially in HAAR and sheared rhyolite. These alterations are associated with U-Zr-mineralizations, which may formed due to a supergene or low-temperature post-magmatic hydrothermal phase, where the precipitation of U, Zr- bearing minerals occurred when the residual late hydrothermal fluids cool to the temperature of meteoric water.

References

- Abd El-Naby, H.H., 2008. Genesis of secondary uranium minerals associated with jasperoid veins, El Erediya area, Eastern Desert Egypt. *Mineralium Deposita* 43 (8), 933-944. <https://doi.org/10.1180/0026461067010311>
- Abdallah, S.E., Azer, M.K., Shammari, A.S.A., 2020. The Petrological and Geochemical Evolution of Ediacaran Rare-Metal Bearing A-type Granites from the Jabal Aja Complex, Northern Arabian Shield, Saudi Arabia. *Acta Geologica Sinica-English Edition* 94 (3), 743-762. <https://doi.org/10.1111/1755-6724.13825>
- Abdel Wahed, A.A.A., Ali, K.G., Khalil, M.M.A., Abdel Gawad, A.E., 2010. Dokhan volcanics of Gabal Monqul area, North Eastern Desert, Egypt: geochemistry and petrogenesis. *Arabian Journal of Geosciences* 5, 29-44. <https://doi.org/10.1007/s12517-010-0136-z>
- Abdel-Rahman, A.M., 2006. Petrogenesis of anorogenic peralkaline granitic complexes from eastern Egypt. *Mineralogical Magazine* 70 (1), 27-50. <https://doi.org/10.1180/0026461067010311>
- Abdelsalam, M.G., Liegeois, J.-P., Stern, R. J., 2002. The Saharan Metacraton. *Journal of African Earth Science* 34 (3-4), 119-136. [https://doi.org/10.1016/S0899-5362\(02\)00013-1](https://doi.org/10.1016/S0899-5362(02)00013-1)
- Abdelsalam, M.G., Stern, R. J., 1996. Sutures and shear zones in the Arabian Nubian Shield. *Journal of African Earth Science* 23 (3), 289-310. [https://doi.org/10.1016/S0899-5362\(97\)00003-1](https://doi.org/10.1016/S0899-5362(97)00003-1)
- Abu Elatta, S.A., Assran, H. M., Ahmed A. A., 2013. Preliminary Study on HFSE Mineralization in the Peralkaline Granites of Nusab El Balgum Area, South Western Desert, Egypt. *Geomaterials* 3, 90-101 <http://dx.doi.org/10.4236/gm.2013.33012>
- Abuamarah, B.A., Azer, M.K., Asimow, P.D., Shi, Q., 2021. Petrogenesis of the post-collisional rare-metal-bearing Ad-Dayheen granite intrusion, Central Arabian Shield. *Lithos* (384-385), 105956. <https://doi.org/10.1016/j.lithos.2020.105956>
- Agrawal, S., 1995. Discrimination between late-orogenic, post-orogenic, and anorogenic granites by major element compositions. *Journal of Geology* 103 (5), 529-537. <http://www.jstor.org/stable/30070775>
- Al-Anazi, E., Al-Saleh, A., 2013. Surface dispersion of uranium in the Al-Hayt area, NE Arabian Shield. *Journal of Environmental Radioactivity* 124, 214-226. <https://doi.org/10.1016/j.jenvrad.2013.05.010>
- Avigad, A., Sandler, A., Kolodner, K., Stern, T.J., McWilliams, M., Miller, N., Beyth, M., 2005. Mass-production of Cambro-Ordovician quartz-rich sandstone as a consequence of chemical weathering of Pan-African terranes: environmental implications. *Earth and Planetary Science Letters* 240 (3-4), 818-826. <https://doi.org/10.1016/j.epsl.2005.09.021>
- Avigad, D. and Gvirtzman, Z., 2009. Late Neoproterozoic rise and fall of the northern Arabian–Nubian Shield: the role of lithospheric mantle delamination and subsequent thermal subsidence. *Tectonophy* 477 (3-4), 217-228. <https://doi.org/10.1016/j.tecto.2009.04.018>
- Avni, Y., Segev, A., Ginat, H., 2012. Oligocene regional denudation of the northern Afar dome: Pre-and syn-breakup stages of the Afro-Arabian plate. *Geological Society of America Bulletin* 124 (11–12), 1871-1897. <https://doi.org/10.1130/B30634.1>
- Azer, M. K., 2013. Late Ediacaran (605–580 Ma) Post-collisional alkaline magmatism in the Arabian-Nubian Shield: A case study of Serbal ring-shaped intrusion, southern Sinai, Egypt. *Journal of Asian Earth Science* 77, 203-223. <https://doi.org/10.1016/j.jseaes.2013.08.029>
- Azer, M.K., 2006. The petrogenesis of late Precambrian felsic alkaline magmatism in South Sinai, Egypt. *Acta Geologica Polonica* 56 (4), 463-484.
- Azer, M.K., Farahat, E.S., 2011. Late Neoproterozoic volcano-sedimentary successions of Wadi Rufaiyil, southern Sinai, Egypt: A case of transition from late- to post-collisional magmatism. *Journal of Asian Earth Sciences* 42 (6), 1187-1203. <https://doi.org/10.1016/j.jseaes.2011.06.016>
- Azer, M.K., Obeid, M.A., Ren, M., 2014. Geochemistry and petrogenesis of late Ediacaran (580–605 Ma) post-collisional alkaline rocks from the Katherina ring complex, south Sinai, Egypt, *Journal of Asian Earth Sciences* 93, 229-252. <https://doi.org/10.1016/j.jseaes.2014.07.028>
- Bachmann, O., and Bergantz, G., 2008. Rhyolites and their source mushes across tectonic settings. *Journal of Petrology* 49 (12), 2277–2285. <https://doi.org/10.1093/petrology/egn068>
- Barbarin, B., 1999. A review of the relationships between granitoid types, their origins, and their geodynamic environments. *Lithos* 46 (3), 605–626. <https://doi.org/10.1016/S0024-4937>
- Barberi, F., Ferrara, G., Santacroce, R., Treuil M, Varet, J., 1975. A transitional basalt- pantellerite sequence of fractional crystallization, the Boina Centre (Afar Rift, Ethiopia). *Journal of Petrology* 16 (1), 22–56. <https://doi.org/10.1093/petrology/16.1.22>
- Barberio, M.R., Donati, C., Donato P., Yirgu G, Peccerillo A., Wu T.W., 1999. Petrology and geochemistry of Quaternary magmatism in the northern sector of the Ethiopian Rift between Debre Zeit and Awash Park. *Acta Vulcanology* 11 (1), 69–81.

- Basta, F.F., Maurice, A.E., Bakhit, B.R., Ali, K.A., Manton, W.I., 2011. Neoproterozoic contaminated MORB of Wadi Ghadir ophiolite, NE Africa: Geochemical and Nd and Sr isotopic constraints. *Journal of African Earth Sciences* 59 (2-3), 227-242. <https://doi.org/10.1016/j.jafrearsci.2010.10.008>.
- Be'eri-Shlevin, Y., Katzir, Y., Valley, J.W., 2009. Crustal evolution and recycling in a juvenile continent: Oxygen isotope ratio of zircon in the northern Arabian Nubian Shield. *Lithos* 107 (3-4), 169-184. <https://doi.org/10.1016/j.lithos.2008.10.001>
- Be'eri-Shlevin, Y., Samuel, M.D., Azer, M.K., Rämö, O.T., Whitehouse, M.J., Moussa, H.E., 2011. The Ediacaran Ferani and Rutig volcano-sedimentary successions of the northernmost Arabian-Nubian Shield (ANS): New insights from zircon U–Pb geochronology, geochemistry and O–Nd isotope ratios. *Precambrian Research* 188 (1-4), 21-44. <https://doi.org/10.1016/j.precamres.2011.04.002>
- Bentor, Y.K., 1985. The crustal evolution of the Arabo-Nubian Massif with special reference to the Sinai Peninsula. *Precambrian research* 28 (1), 1-74. [https://doi.org/10.1016/0301-9268\(87\)90008-8](https://doi.org/10.1016/0301-9268(87)90008-8)
- Bevins, R.E., Pharaoh, T.C., Cope, J.C.W., Brewer, T.S., 1995. Geochemical character of Neoproterozoic volcanic rocks in southwest Wales. *Geological Magazine* 132 (3), 339-349. <https://doi.org/10.1017/S0016756800013649>
- Boctor, N.Z., Yoder, H.S.Jr., 1986. Petrology of some melilite-bearing rocks from Cape Province, Republic of South Africa: relationship to kimberlite. *American Journal of Sciences* 286 (7), 513-539. <https://doi.org/10.2475/ajs.286.7.513>
- Bonin, B., 2007. A-type granites and related rocks: Evolution of a concept, problems and prospects. *Lithos* 97 (1–2), 1-29. <https://doi.org/10.1016/j.lithos.2006.12.007>
- Bonin, B., Janoušek, V., Moyen, J.F., 2020. Chemical variation, modal composition and classification of granitoids. *Geological Society, London, Special Publications* 491 (1), 9-51. <https://doi.org/10.1144/SP491-2019-138>
- Bosworth, W., Huchon, P., McClay, K., 2005. The Red Sea and Gulf of Aden Basins. *Journal of African Earth Sciences* 43, 334–378. <https://doi.org/10.1016/j.jafrearsci.2005.07.020>
- Camp, V.E. and Roobol, M.J., 1992. Upwelling asthenosphere beneath western Arabia and its regional implications. *Journal of Geophysical Research* 97 (B11), 15255-15271. <https://doi.org/10.1029/92JB00943>
- Chalot-Prat, F., 1995. Genesis of rhyolitic ignimbrites and lavas from district sources at a deep crustal level: field, petrographic, chemical, and isotopic (Sr, Nd) constraints in the Tazekka volcanic complex (Eastern Morocco). *Lithos* 36 (1), 29-49. [https://doi.org/10.1016/0024-4937\(95\)00004-Y](https://doi.org/10.1016/0024-4937(95)00004-Y)
- Chazot, G., Bertrand, H., 1995. Genesis of silicic magmas during Tertiary continental rifting in Yemen. *Lithos* 36 (2), 69-83. [https://doi.org/10.1016/0024-4937\(95\)00012-5](https://doi.org/10.1016/0024-4937(95)00012-5)
- Christiansen, E.H., 2005. Contrasting processes in silicic magma chambers: Evidence from very large volume ignimbrites. *Geological magazine* 142 (6), 669–681. <https://doi.org/10.1017/S0016756805001445>
- Christiansen, E.H., McCurry, M., 2008. Contrasting origins of Cenozoic silicic volcanic rocks from the western Cordillera of the United States. *Bulletin of Volcanology* 70, 251–267 <https://doi.org/10.1007/s00445-007-0138-1>
- Collins, W.J., Beams, S.D., White, A.J.R., and Chappell, B.W., 1982. Nature and origin of A-type granites with particular reference to South-eastern Australia, *Contributions to Mineralogy and Petrology* 80 (2), 189–200. <https://doi.org/10.1007/BF00374895>
- Collins, W.J., Huang, H.Q., Bowden, P., Kemp, A.I.S., 2019. Repeated S–I–A-type granite trilogy in the Lachlan Orogen and geochemical contrasts with A-type granites in Nigeria: Implications for petrogenesis and tectonic discrimination. In Janoušek, V., Bonin, B., Collins, W.J., Farina, F., and Bowden, P. (Eds.): *Post-Archean Granitic Rocks: Petrogenetic Processes and Tectonic Environments*. Geological Society, London, Special Publications, 491. <https://doi.org/10.1144/SP491-2018-159>
- Corti, G., 2009. Continental rift evolution: from rift initiation to incipient break-up in the Main Ethiopian Rift, East Africa. *Earth-Science Reviews* 96, 1–53 <http://dx.doi.org/10.1016/j.earscirev.2009.06.005>
- Coulon, C., Dostal, J., Dupuy, C., 1978. Petrology and geochemistry of the ignimbrites and associated lava domes from N. W. Sardinia. *Contribution to Mineralogy and Petrology* 68 (1), 89-98. <https://doi.org/10.1007/BF00375450>
- Dall'Agnol, R., Scaillet, B., Pichavant, M., 1999. An experimental study of a lower Proterozoic A-type granite from the eastern Amazonian Craton, Brazil. *Journal of Petrology* 40 (11), 1673-1698. <https://doi.org/10.1093/ptroj/40.11.1673>
- Davies, J. H. and von Blanckenburg, F., 1995. Slab breakoff: A model of lithosphere detachment and its test in the magmatism and deformation of collisional orogens. *Earth and Planetary Science Letters* 129 (1-4), 85-102. [https://doi.org/10.1016/0012-821X\(94\)00237-S](https://doi.org/10.1016/0012-821X(94)00237-S)
- Dawood, Y.H., Abd El-Naby, H.H., 2022. Genesis of uranyl mineralization in the Arabian Nubian Shield: A review. *Journal of Asian Earth Sciences* 225, 105047. <https://doi.org/10.1016/j.jseaes.2021.105047>

- Dawood, Y.H., Abd El-Naby, H.H., Ghaleb, B., 2014. U-series isotopic composition of kasolite associated with aplite-pegmatite at Jabel Sayid, Hijaz region, Kingdom of Saudi Arabia. *Arabian Journal of Geosciences* 7, 2881–2892. <https://doi.org/10.1007/s12517-013-0963-9>
- Deering, C.D., Gravley, D.M., Vogel, T.A., Cole, J.W., and Leonard, G.S., 2010. Origins of cold wet-oxidizing to hot- dry-reducing rhyolite magma cycles and distribution in the Taupo Volcanic Zone, New Zealand. *Contribution Mineralogy and Petrology* 160, 609-629. <https://doi.org/10.1007/s00410-010-0496-0>
- Eby, G.N., 1990. The A-type granitoids: A review of their occurrence and chemical characteristics and speculations on their petrogenesis. *Lithos* 26 (1-2), 115-134. [https://doi.org/10.1016/0024-4937\(90\)90043-Z](https://doi.org/10.1016/0024-4937(90)90043-Z)
- Eby, G.N., 1992. Chemical subdivision of the A-type granitoids: petrogenetic and tectonic implications. *Geology* 20 (7), 641-644. [https://doi.org/10.1130/0091-7613\(1992\)020](https://doi.org/10.1130/0091-7613(1992)020)
- El-Bialy, M.Z., Zoheir, B.A., Koutsovitis, P., Feigenson, M., Omar, M.M., 2022. The anorogenic late Ediacaran granite-rhyolite porphyries of Gabal Abu Durba, Sinai: termination of magmatism in the Neoproterozoic Arabian-Nubian Shield crust. *International Geology Review* 1-40. <https://doi.org/10.1080/00206814.2022.2079009>
- El-Bialy, M.Z. and Hassan, I.S., 2012. The late Ediacaran (580-590Ma) onset of anorogenic alkaline magmatism in the Arabian–Nubian Shield: Katherina A-type rhyolites of Gabal Ma'ain, Sinai, Egypt. *Precambrian Research*, (216-219), 1-22. <https://doi.org/10.1016/j.precamres.2012.06.004>
- El-Bialy, M.Z., 2013. Geochemistry of the Neoproterozoic metasediments of Malhaq and Um Zariq formations, Kid metamorphic complex, Sinai, Egypt: Implications for source-area weathering, provenance, recycling, and depositional tectonic setting. *Lithos* 175–176, 68-85. <https://doi.org/10.1016/j.lithos.2013.05.002>
- Eliwa, H.A., Breitmeyer, C., Murata, M., Khalaf, I.M., Bühler, B., Itaya, T., Takahashi, T., Hirahara, Y., Miyazaki, T., Kimura, J.I., Shibata, T., Koshi, Y., Kato, Y., Ozawa, H., Daas, M.A., El Gameel, K., 2014. SIMS zircon U-Pb and mica K-Ar geochronology, and Sr-Nd isotope geochemistry of Neoproterozoic granitoids and their bearing on the evolution of the north Eastern Desert, Egypt. *Gondwana Research* 25 (4), 1570-1598. <https://doi.org/10.1016/j.gr.2013.06.006>
- Elwan, W., 2019. Petrogenesis of Homrat El-Girigab alkali-feldspar granites, northern Eastern Desert, Egypt. *Egyptian Journal of Geology* 63 (1), 307-324. <https://doi.org/10.21608/egj.2019.216358>
- Elwan, W., Azzaz, S.A., Balasi, M.R and Amer, O., 2019. Petrogenesis of Maktali fractionated calc-alkaline younger granitoids, Central Eastern Desert, Egypt. *Arabian Journal of Geosciences* 12, 393. <https://doi.org/10.1007/s12517-019-4559-x>
- Evensen, N.M., Hamilton, P.J., O' Nions, R.K., 1978. Rare earth abundances in chondritic meteorites. *Geochimica et Cosmochimica Acta* 42(8), 1199-1212. [https://doi.org/10.1016/0016-7037\(78\)90114-X](https://doi.org/10.1016/0016-7037(78)90114-X)
- Eyal, M., Litvinovsky, B., Jahn, B.M., Zanvilevich, A. and Katzir, Y., 2010. Origin and evolution of post-collisional magmatism: Coeval Neoproterozoic calc-alkaline and alkaline suites of the Sinai Peninsula. *Chemical Geology* 269 (3-4), 153-179. <https://doi.org/10.1016/j.chemgeo.2009.09.010>
- Farahat, E., Zaki, R., Hauenberger, C. Mabrouk S. 2011. Neoproterozoic calc-alkaline peraluminous granitoids of the Delehimmi pluton, Central Eastern Desert, Egypt: Implications for transition from late- to post-collisional tectonomagmatic evolution in the northern Arabian-Nubian Shield. *Geological Journal* 46 (6), 544-560 <https://doi.org/10.1002/gj.1289>
- Farahat, E.S., Mohamed, H.A., Ahmed, A.F., El Mahallawi, M.M., 2007. Origin of I and A-type granitoids from the Eastern Desert of Egypt: implications for crustal growth in the northern Arabian-Nubian Shield. *Journal of African Earth Sciences* 49 (1-2), 43-58. <https://doi.org/10.1016/j.jafrearsci.2007.07.002>
- Farahat, E.S., Azer, M.K., 2011. Post-collisional magmatism in the northern Arabian-Nubian Shield: The geotectonic evolution of the alkaline suite at Gebel Tarbush area. south Sinai, Egypt. *Chemie der Erde*, 71 (3), 247-266. <https://doi.org/10.1016/j.chemer.2011.06.003>
- Frost, B.R., Barnes, C.G., Collins, W.J., Arculus, R.J., Ellis, D.J., and Frost, C.D., 2001. A geochemical classification for granitic rocks. *Journal of Petrology* 42 (11): 2033-2048. <https://doi.org/10.1093/petrology/42.11.2033>
- Frost, B.R., Frost, C.D., 2008. A geochemical classification for feldspathic rocks. *Journal of Petrology* 49 (11), 1955-1969. <https://doi.org/10.1093/petrology/egn054>
- Frost, C.D., and Frost, B.R., 2011. On Ferroan (A-type) Granitoids: Their Compositional Variability and Modes of Origin, *Journal of Petrology* 52 (1), 39–53. <https://doi.org/10.1093/petrology/egq070>
- Frost, C.D., Frost, B.R., and Beard, J.S., 2016. On silica-rich granitoids and their eruptive equivalents. *American Mineralogist* 101 (6), 1268-1284. <https://doi.org/10.2138/am-2016-5307>
- Gaafar, I., Cuney, M., Gawad, A.A., 2014. Mineral Chemistry of Two-Mica Granite Rare Metals: Impact of Geophysics on the Distribution of Uranium Mineralization at El Sela Shear Zone Egypt. *Open Journal of Geology* 4 (4), 137–160. <https://doi.org/10.4236/ojg.2014.44011>

- Gahlan, H.A., Asimow, P.D., Azer, M.K., Ma, C., Al-Kahtany, K.M., Hakeem, A.Y., 2021. Geochemistry and mineralogy of the Jebel Aja Igneous Intrusion and the associated exotic pegmatites, Arabian Shield, Saudi Arabia. *Lithos* (400-4001),106395. <https://doi.org/10.1016/j.lithos.2021.106395>
- Gahlan, H.A., Azer, M.K., Al-Hashim, M.H., Heikal, M.T.S., 2022. Highly evolved rare-metal bearing granite overprinted by alkali metasomatism in the Arabian Shield: A case study from the Jabal Tawlah granites. *Journal of African Earth Sciences* 92, 104556. <https://doi.org/10.1016/j.jafrearsci.2022.104556>
- Garfunkel, Z. and Ban-Avraham Z., 2001. Basins along the Dead Sea Transform. In: Ziegler, P.A., Cavazza, W., Robertson A.H.F., Crasquin-Soleau S. (eds.): Peri-Tethys Memoir 6: Peri Tethyan rift/wrench basins and passive margins, Mémoires du Muséum national d'histoire naturelle 186. Publications Scientifiques du Muséum, Paris, 607–627. ISBN 10: 2856535283.
- Gill, J.B., 1981. Orogenic andesites and plate tectonics. Springer-Verlag Berlin, Heidelberg, 392p. <https://doi.org/10.1007/978-3-642-68012-0>
- Grant, J.A., 1986. The isocon diagram—a simple solution to Gresens equation for metasomatic alteration. *Economic Geology* 81 (8): 1976–1982. <https://doi.org/10.2113/gsecongeo.81.8.1976>
- Grebennikov, A.V., 2014. A-type granites and related rocks: Petrogenesis and classification. *Russian Geology and Geophysics* 55 (11), 1353-1366. <https://doi.org/10.1016/j.rgg.2014.10.011>
- Green, T.H., 1980. Island arc and continent-building magmatism: A review of petrogenetic models based on experimental petrology and geochemistry. *Tectonophysics* 63 (1-4), 367-385. [https://doi.org/10.1016/0040-1951\(80\)90121-3](https://doi.org/10.1016/0040-1951(80)90121-3)
- Green, M. G., Sylvester, P. J., Buick, R., 2000. Growth and recycling of early Archaean continental crust: geochemical evidence from the Coonterunah and Warrawoona Groups, Pilbara Craton, Australia. *Tectonophysics* 322, 69-88.
- Hadj-Kaddour, Z., Liegeois, J-P, Demaiffe, D., Caby, R., 1998. The alkaline-peralkaline granitic post-collisional Tin Zibane dyke swarm (Pan-African Tuareg shield, Algeria): prevalent mantle signature and late apatitic differentiation. *Lithos* 45, 223-243. [https://doi.org/10.1016/S0024-4937\(98\)00033-4](https://doi.org/10.1016/S0024-4937(98)00033-4)
- Hadley, D.G.; Schmidt, D.L., 1980. Sedimentary rocks and basins of the Arabian Shield and their evolution. In: Cooray, P.G.; Tahoun, S.A. (eds.) *Evolution and Mineralization of the Arabian-Nubian Shield*. Institute of Applied Geology, Jiddah, Bulletin 3, Pergamon Press 4, 25-50
- Hanson, G.N., 1978. The application of trace elements to the petrogenesis of igneous rocks of granitic composition. *Earth and Planetary Science Letters* 38 (1), 26-43. [https://doi.org/10.1016/0012-821X\(78\)90124-3](https://doi.org/10.1016/0012-821X(78)90124-3)
- Harris, N.B.W., 1982. The petrogenesis of alkaline intrusives from Arabia and Northeast Africa and their implications for within-plate magmatism. *Tectonophysics* 83 (3-4), 243-258. [https://doi.org/10.1016/0040-1951\(82\)90021-X](https://doi.org/10.1016/0040-1951(82)90021-X)
- Hecht, L., Thuro K., Plinninger, R. Cuney, M., 1999. Mineralogical and geochemical characteristics of hydrothermal alteration and episyenitization in the Königshain granites, northern Bohemian Massif, Germany. *International Journal of Earth Sciences* 88, 236-252. <https://doi.org/10.1007/s005310050262>
- Hofmann, A.W., 1997, Mantle geochemistry: The message from oceanic volcanism, *Nature* 385 (6613), 219–229. <https://doi.org/10.1038/385219a0>
- Huang, H., Niu, Y., Zhao, Z., Hei, H., and Zhu, D., 2011, On the enigma of Nb-Ta and Zr-Hf fractionation - A critical review. *Journal of Earth Science* 22 (1), 52-66. <https://doi.org/10.1007/s12583-011-0157-x>
- Ibrahim, M.E., Saleh, G.M., Dawood, M.I., Kamar, M.S., Saleh, S.M., Mahmoud, M.A., El-Tohamy, A.M., 2017. Rare Metals Mineralization in Pegmatite at Abu Rusheid Area, South Eastern Desert Egypt. *International Journal of Mining Sciences* 3 (1), 44–63. <http://dx.doi.org/10.20431/2454-9460.0301004>
- Irber, W., 1999. The lanthanide tetrad effect and its correlation with Eu/Eu*, Y/Ho and Zr/Hf for evolving peraluminous granitic suites. *Geochimica Cosmochimica Acta* 63 (3-4),489-508. [https://doi.org/10.1016/S0016-7037\(99\)00027-7](https://doi.org/10.1016/S0016-7037(99)00027-7)
- Jahn, B., Wu, F., Capdevila, R. and Martineau, F., 2001. Highly evolved juvenile granites with REE tetrad pattern: the Woduhe and Baerzhe granites from the Great Xing'an Mountains in NE China. *Lithos* 59 (4), 171-198. [https://doi.org/10.1016/S0024-4937\(01\)00066-4](https://doi.org/10.1016/S0024-4937(01)00066-4)
- Jarrar, G.H., Manton, W.I., Stern, R.J., Zachmann, D., 2008. Late Neoproterozoic A-type granites in the northernmost Arabian-Nubian Shield formed by fractionation of basaltic melts. *Geochemistry* 68 (3): 295-312. <https://doi.org/10.1016/j.chemer.2006.09.002>
- Johnson P.R, Halverson G.P, Kusky T.M, Stern R.J, Pease, V., 2013. Volcanosedimentary Basins in the Arabian-Nubian Shield: markers of repeated exhumation and denudation in a Neoproterozoic accretionary orogen. *Geosciences* 3 (3), 389-445. <https://doi.org/10.3390/geosciences3030389>

- Johnson P.R., 2003. Post-amalgamation basins of the NE Arabian shield and implications for Neoproterozoic III tectonism in the northern East African orogen. *Precambrian Research* 123 (2-4), 321–337. [https://doi.org/10.1016/S0301-9268\(03\)00074-3](https://doi.org/10.1016/S0301-9268(03)00074-3)
- Johnson, P.R., Andresen, A., Collins, A.S., Fowler, A.R., Fritz, H. Ghebreab, W., Kusky, T. and Stern, R.J., 2011. Late Cryogenian- Ediacaran history of the Arabian-Nubian Shield: a review of deposition, plutonic, structural, and tectonic events in the closing stages of the northern East African Orogen. *Journal African Earth Science*, 61(3), 167-232. <https://doi.org/10.1016/j.jafrearsci.2011.07.003>
- Johnson, P.R., 2006. Explanatory Notes to the Map of Proterozoic Geology of Western Saudi Arabia. Saudi Geological Survey Technical Report SGS-TR-2006-4, p. 62, 22 figures., 2 plates.
- Jung, S, Pfänder, J.A., 2007. Source composition and melting temperatures of orogenic granitoids: constraints from CaO/Na₂O, Al₂O₃/TiO₂ and accessory mineral saturation thermometry. *European Journal of Mineralogy*, 19, 859–870. <https://doi.org/10.1127/0935-1221/2007/0019-1774>
- Kamber, B.S., Collerson, K.D., 2000. Role of hidden subducted slabs in mantle depletion. *Chemical Geology* 166 (3-4), 241–254. [https://doi.org/10.1016/S0009-2541\(99\)00218-1](https://doi.org/10.1016/S0009-2541(99)00218-1)
- Kemp, A.I.S., Wormald, R.J., Whitehouse, M.J., Price, R.C., 2005. Hf isotopes in zircon reveal contrasting sources and crystallization histories for alkaline to peralkaline granites of Temora, southeastern Australia. *Geology* 33 (10), 797-800. <https://doi.org/10.1130/G21706.1>
- Kemp, J., 1998. Caldera-related volcanic rocks in the Shammar group, northern Arabian Shield. *Journal of African Earth Sciences* 26 (4), 551-572. [https://doi.org/10.1016/S0899-5362\(98\)00033-5](https://doi.org/10.1016/S0899-5362(98)00033-5)
- Kessel, R., Stein, M., Navon, O., 1998. Petrogenesis of late Neoproterozoic dikes in the northern Arabian-Nubian Shield: Implications for the Origin of A-type granites. *Precambrian Research* 92 (2), 195-213. [https://doi.org/10.1016/S0301-9268\(98\)00075-8](https://doi.org/10.1016/S0301-9268(98)00075-8)
- Khalil, A.E.S., Obeid, M.A., Azer, M.K., Asimow, P.D., 2018. Geochemistry and petrogenesis of post-collisional alkaline and peralkaline granites of the Arabian-Nubian Shield: a case study from the southern tip of Sinai Peninsula, Egypt. *International Geology Review* 60 (8), 998-1018. <https://doi.org/10.1080/00206814.2017.1364672>
- Kouske, A., Suh, C., Ghogomu, R., Ngako, V., 2012. Na-Metasomatism and Uranium Mineralization during a Two-Stage Albitization at Kitongo, Northern Cameroon: Structural and Geochemical Evidence," *International Journal of Geosciences* 3 (1), 258-279. [doi: 10.4236/ijg.2012.31028](https://doi.org/10.4236/ijg.2012.31028).
- Kuibida, M.L., Murzin, O.V., Kruk, N.N., Naryzhnova, A.V. et al., 2020. Whole-rock geochemistry and U-Pb ages of Devonian bimodal-type rhyolites from the Rudny Altai, Russia: Petrogenesis and tectonic settings. *Gondwana Research* 81, 312-338. <https://doi.org/10.1016/j.gr.2019.12.002>
- Liégeois, J.P., Navez, J., Hertogen, J., and Black, R., 1998. Contrasting origin of post-collisional high-K calc-alkaline and shoshonitic versus alkaline and peralkaline granitoids. The use of sliding normalization, *Lithos* 45 (1–4), 1–28. [https://doi.org/10.1016/S0024-4937\(98\)00023-1](https://doi.org/10.1016/S0024-4937(98)00023-1)
- Liégeois, J.P., Black, R., 1987. Alkaline magmatism subsequent to collision in the Pan-African belt of the Adrar des Iforas (Mali). In: Fitton J.G., Upton, B.G.J. (eds): *Alkaline igneous rocks*. Geological Society of London Special Publication 30 (1), 381-401. <https://doi.org/10.1144/GSL.SP.1987.030.01.18>
- Laurent, O., Martin, H., J.F., Moyen, J.F., Doucelance, R., 2014. The diversity and evolution of late-Archean granitoids: Evidence for the onset of “modern-style” plate tectonics between 3.0 and 2.5 Ga. *Lithos* 205, 208-235. [http://dx.doi.org/10.1016/j.lithos.2014.06.012](https://dx.doi.org/10.1016/j.lithos.2014.06.012) Liégeois, J.P., Navez, J., Hertogen, J., and Black, R., 1998. Contrasting origin of post-collisional high-K calc-alkaline and shoshonitic versus alkaline and peralkaline granitoids. The use of sliding normalization, *Lithos* 45, (1–4), 1–28. [https://doi.org/10.1016/S0024-4937\(98\)00023-1](https://doi.org/10.1016/S0024-4937(98)00023-1)
- Le Maitre, R.W., Bateman, P., Dudek, A., Keller, J., Lameyre, J., Le Bas, M. J., Sabine, P. A., Schmid, R., Sorensen, H., Streckeisen, A., Woolley, A. R. and Zanettin, B., 1989. A classification of igneous rocks and glossary of terms: Recommendations of the International Union of Geological Sciences Subcommission on the Systematics of Igneous Rocks. Blackwell, Oxford, 193pp.
- Liu, Y., Diwu, C., Zhao, Y. Xiaoming, L., Yuan, H and Wang, H., 2014. Determination of trace and rare-earth elements in Chinese soil and clay reference materials by ICP-MS. *Chinese Journal of Geochemistry*, 33(1), 95-102. <https://doi.org/10.1007/s11631-014-0663-5>
- logical results. *International Journal of Earth Sciences* 109 (1), 101–125. <https://doi.org/10.1007/s00531-019-01791-x>
- Macdonald, R., 1974. Nomenclature and petrochemistry of the peralkaline oversaturated extrusive rocks. *Bulletin of Volcanology* 38, 498–516. <https://doi.org/10.1007/BF02596896>
- Macdonald, R., Belkin, H.E., Fitton, J.G., Rogers, N.W., Nejbort, K., Tindle, A.G, Marshall, A.S., 2008. The roles of fractional crystallization, magma mixing, crystal mush remobilization and volatile-melt interactions in the genesis of a young basalt-peralkaline rhyolite suite, the Greater Olkaria Volcanic

- Complex, Kenya Rift Valley. *Journal of Petrology* 49 (8):1515–1547. <https://doi.org/10.1093/petrology/egn036>
- Maniar, P.D., Piccoli, P.M., 1989. Tectonic discrimination of granitoids. *Geological society of America Bulletin* 101 (5), 635-643. [https://doi.org/10.1130/0016-7606\(1989\)101](https://doi.org/10.1130/0016-7606(1989)101)
- Martin, R.F., 2006. A-type granites of crustal origin ultimately results from open-system fenitization-type reactions in an extensional environment. *Lithos* 91 (1–4), 125-136. <https://doi.org/10.1016/j.lithos.2006.03.012>
- McKay, G.A., 1989. Partitioning of rare earth elements between major silicate minerals and basaltic melts. *Reviews in Mineralogy and Geochemistry* 21 (1),45-77. <https://doi.org/10.1515/9781501509032-006>
- Moghazi, A.M., Harbi H.M., Ali, K.A., 2011. Geochemistry of the Late Neoproterozoic Hadb adh Dayheen ring complex, Central Arabian Shield: implications for the origin rare-metal-bearing post-orogenic A-type granites. *Journal of Asian Earth Science* 42 (6), 1324-1340. <https://doi.org/10.1016/j.jseaes.2011.07.020>
- Mohamed, F., Moghazi, A., Hassanen, M., 2000. Geochemistry, petrogenesis and tectonic setting of late Neoproterozoic Dokhan-type volcanic rocks in the Fatira area, eastern Egypt. *International Journal of Earth Sciences* 88, 764-777. <https://doi.org/10.1007/s005310050304>
- Möller, P., Bau, M., 1993. Rare-earth patterns with positive cerium anomaly in alkaline waters from Lake Van, Turkey. *Earth Planetary Science Letters* 117 (3-4), 671–676. [https://doi.org/10.1016/0012-821X\(93\)90110-U](https://doi.org/10.1016/0012-821X(93)90110-U)
- Moore, J.M., 1978. Volcanogenic mineralization and a rhyolite dome in the Arabian Shield. *Mineralium Deposita* 13, 123-129. <https://doi.org/10.1007/BF00202912>
- Moufti, M. R., Moghazi, A. M. and Ali, K. A., 2012. Geochemistry and Sr-Nd-Pb isotopic composition of the Harrat Al-Madinah Volcanic Field, Saudi Arabia. *Gondwana Research* 21 (2-3), 670–689. <https://doi.org/10.1016/j.gr.2011.06.003>
- Mushkin, A., Navon, O., Halicz, L., Heimann, A., Woerner, G Stein, M., 1999. Geology and geochronology of the Amram Massif, southern Negev Desert, Israel. *Israel Journal of Earth Sciences* 48, 179-193.
- Ohta, T., & Arai, H., 2007. Statistical empirical index of chemical weathering in igneous rocks: a new tool for evaluating the degree of weathering. *Chemical Geology*, 240 (3-4), 280-297. <https://doi.org/10.1016/j.chemgeo.2007.02.017>
- Patchett, P. J., & Chase, C. G., 2002. Role of transform continental margins in major crustal growth episodes. *Geology*, 30 (1), 39–42. [https://doi.org/10.1130/0091-7613\(2002\)030<0039:ROTCMI>2.0.CO;2](https://doi.org/10.1130/0091-7613(2002)030<0039:ROTCMI>2.0.CO;2)
- Perfit, M.R., Gust, D.A., Bence, A.E., Arculus, R.J., Taylor, S.R., 1980. Chemical characteristics of island-arc basalts: Implications for mantle sources. *Chemical Geology* 30 (3), 227-256. [https://doi.org/10.1016/0009-2541\(80\)90107-2](https://doi.org/10.1016/0009-2541(80)90107-2)
- Quick, J.E., Doebrich, J.L, 1987. Geologicmap of theWadiAsh Shu’bah quadrangle, sheet 26 Kingdom of Saudi Arabia (with text): Saudi Arabian Directorate General of Mineral Resources, Geoscience Map GM-108
- Ragland, P.C., 1989. Basic analytical petrology. Oxford University Press, New York, 369p. ISBN: 0195045343, 0195045351.
- Rapp, R.P., and Watson, E.B., 1995. Dehydration melting of metabasalt at 8-32 kbar: Implications for continental growth and crust–mantle recycling, *Journal of Petrology* 36 (4), 891–931. <https://doi.org/10.1093/petrology/36.4.891>
- Robinson, F.A., Foden, J.D., Collins, A.S. and Payne, J.L., 2014. Arabian Shield magmatic cycles and their relationship with Gondwana assembly: Insights from zircon U–Pb and Hf isotopes. *Earth and Planetary Science Letters* 408, 207-225. <https://doi.org/10.1016/j.epsl.2014.10.010>
- Rollinson, H., 1994. Using geochemical data: evaluation, presentation, interpretation. Longman Scientific & Technical - John Wiley & Sons Inc. New York, 352 pp.
- Rudnick, R.L. and Gao, S. 2003. The Composition of the Continental Crust. In: Holland, H.D. and Turekian, K.K., (eds.). *Treatise on Geochemistry*, 3, The Crust, Elsevier-Pergamon, Oxford, 1-64. <http://dx.doi.org/10.1016/b0-08-043751-6/03016-4>
- Rudnick, R.L., Fountain, D.M., 1995. Nature and composition of the continental crust: A lower crustal perspective. *Reviews in Geophysics*, 33 (3), 267–309. <https://doi.org/10.1029/95RG01302>
- Saleh, G.M., Kamar, M.S., Mira, H.I, 2021. Phanerozoic Minor Volcanics and Intrusives of the Arabian-Nubian Shield. In: Hamimi, Z., Fowler, A.-R., Liegeois, J.-P., Collins, A., Abdelsalam, M., Abd EI-Wahed, M. (eds.). *The Geology of the Arabian-Nubian Shield*. Regional Geology Reviews. https://doi.or/10.1007/978-3-030-72995-0_26
- Salih, M.A., Abdallsamed, M.I.M., Ma, C.Q., Mustafa, H.A., Ahmed, H.A., Wang, L.X., 2020. Genesis of alkaline-peralkaline A-type granite from El Dair complex SW Arabian- Nubian Shield, Sudan: Geochronology, geochemistry and isotopic constraints. *Arabian Journal of Geosciences* 13 (1), 42. <https://doi.org/10.1007/s12517-019-5034-4>

- Salih, M.O., Abdel Rahman, E.M., 2021. Geology, geochemistry, and petrogenesis of Jebal Ruro A-type granite, Blue Nile State, Sudan: Implications for origin of HFSE mineralization. *Arabian Journal of Geosciences* 14 (11), 958. <https://doi.org/10.1007/s12517-021-07283-0>
- Samuel, M.D., Mousa, H.E., and Azer, M.K., 2007. A-type volcanics in Central Eastern Sinai, Egypt. *Journal of African Earth Sciences*, 47 (4-5): 203-226. <https://doi.org/10.1016/j.jafrearsci.2007.02.006>
- Schandl, E.S., Gorton, M.P., 2002. Application of high field strength elements to discriminate tectonic settings in VMS environments. *Economic Geology* 97 (3), 629-642. <https://doi.org/10.2113/gsecongeo.97.3.629>
- Seddik, A.M.A., Darwish, M.H., Azer, M.K., Asimow, P.D., 2020. Assessment of magmatic versus post-magmatic processes in the Mueilha rare-metal granite, Eastern Desert of Egypt. *Arabian-Nubian Shield. Lithos* (366-367), 105542. <https://doi.org/10.1016/j.lithos.2020.105542>
- Shalaby, M.H., Abu Zeid, E.K., Mahdy, N.M., 2015. On the petrogenesis and evolution of U-rich granite: insights from mineral chemistry studies of Gattar granite, North Eastern Desert Egypt. *Arabian Journal of Geosciences* 8 (6), 3565–3585. <https://doi.org/10.1007/s12517-014-1466-z>
- Shellnutt, J.G., Wang, C.Y., Zhou, M.F., Yang, Y., 2009. Zircon Lu–Hf isotopic compositions of metaluminous and peralkaline A-type granitic plutons of the Emeishan large igneous province (SW China): Constraints on the mantle source. *Journal of Asian Earth Sciences* 35 (1), 45-55. <https://doi.org/10.1016/j.jseaes.2008.12.003>
- Sherif, M.I., Ghoneim, M.F., Heikal, M.T.S., El Dosuky, B.T., 2013. Petrogenesis of granites, Sharm El-Sheikh area, South Sinai, Egypt: petrological constrains and tectonic evolution. *Mineralogy and petrology* 107 (5), 765–783. <https://doi.org/10.1007/s00710-013-0267-5>
- Stein, M. and Hofmann, A.W., 1992. Fossil plume head beneath the Arabian lithosphere? *Earth and Planetary Science Letters* 114 (1): 193-209. [https://doi.org/10.1016/0012-821X\(92\)90161-N](https://doi.org/10.1016/0012-821X(92)90161-N)
- Stern, R. J., 1994. Arc assembly and continental collision in the Neoproterozoic East African Orogen: implications for consolidation of Gondwanaland. *Annual Review of Earth and Planetary Sciences* 22, 319-351. <https://doi.org/10.1146/ANNUREV.EA.22.050194.001535>
- Stern, R. J., 2002. Crustal evolution in the East African Orogen: a neodymium isotopic perspective. *Journal of African Earth Science* 34 (3-4), 109-117. [https://doi.org/10.1016/S0899-5362\(02\)00012-X](https://doi.org/10.1016/S0899-5362(02)00012-X)
- Stern, R. J., 2008. Neoproterozoic crustal growth: the solid Earth system during acritical episode of the Earth history. *Gondwana Research* 14 (1-2), 33-50. <https://doi.org/10.1016/j.gr.2007.08.006>
- Stern, R.J., Gottfried, D., 1986. Petrogenesis of late Precambrian (575–600 Ma) bimodal suite in northeast Africa. *Contributions to Mineralogy and Petrology* 92 (4), 492–501. <https://doi.org/10.1007/BF00374431>
- Stern, R.J., Hedge, C.E., 1985. Geochronologic and isotopic constraints on late Precambrian crustal evolution in the Eastern Desert of Egypt. *American Journal of Sciences* 285 (2), 97-127. <https://doi.org/10.2475/ajs.285.2.97>
- Stoeser, D. B., Frost, C. D., 2006. Nd, Pb, Sr, and O isotopic characterization of Saudi Arabian Shield terranes. *Chemical Geology* 226 (3-4), 163-188. <https://doi.org/10.1016/j.chemgeo.2005.09.019>
- Stuckless, J.S., Hedge, C.E., Wenner, D.B. and Nkomo, I.T., 1984. Isotopic studies of post orogenic granites from the northeastern Arabian Shield. Kingdom of Saudi Arabia: Saudi Arabian Deputy Ministry for Mineral Resources Open-File Report USGS-04-42, 40 p.
- Sun, S., McDonough, W.F., 1989. Chemical and isotopic systematic of oceanic basalts: implications for mantle compositions and processes. *Magmatism in the Ocean Basins*: In: Saunders, A.D, Norry M.J., (eds.). Geological Society of London, Special Publications 42 (1), 313-345. <https://doi.org/10.1144/GSL.SP.1989.042.01.19>
- Sylvester, P.J., 1989. Post-collisional alkaline granites. *Journal of Geology* 97(3), 261-280. <https://www.jstor.org/stable/30068745>
- Szemerédi, M., Lukacs, R., Varga, A., Dunkl, I. et al., 2020. Permian felsic volcanic rocks in the Pannonian Basin (Hungary): New petrographic, geochemical, and geochronological results. *International Journal of Earth Sciences* 109 (1), 101-125. <https://doi.org/10.1007/s00531-019-01791-x>
- Taylor, S. R. and McLennan, S. M. 1985. *The continental crust: its composition and evolution*. Oxford, England: Blackwell Scientific Publications. ISBN-13: 978-0632011483, 312 p.
- Trua T, Deniel C, Mazzuoli R (1999) Crustal control in the genesis of Plio-Quaternary bimodal magmatism of the Main Ethiopian Rift (MER): geochemical and isotopic (Sr, Nd, Pb) evidence. *Chemical Geology* 155 (3-4), 201–231. [https://doi.org/10.1016/S0009-2541\(98\)00174-0](https://doi.org/10.1016/S0009-2541(98)00174-0)
- Ulrych J., Povondra P., Huspeka J., Pivec E., Rutšek J., 1990. Chemical composition of melilitic volcanics of northern part of the Bohemian Massif. Report of the Projects II-4-1/07 and II/4/4/05. Institute of Geosciences, Faculty of Science, Charles University, Prague, 1-123 (in Czech).

- Wittke, J.H., and Mack, L.E., 1993. OIB-Like Mantle Source for Continental Alkaline Rocks of the Balcones Province, Texas: Trace-Element and Isotopic Evidence, *Journal of Geology* 101 (3), 333-344. <https://doi.org/10.1086/648227>
- Weaver, B.L., 1991. The origin of ocean island basalts end-member compositions: trace elements and isotopic constraints. *Earth and Planetary Science Letters* 104 (2-4), 381-397. [https://doi.org/10.1016/0012-821X\(91\)90217-6](https://doi.org/10.1016/0012-821X(91)90217-6)
- Wedepohl, K.H., 1994. The composition of the continental crust. *Geochimica et Cosmochimica Acta* 59 (7), 1217-1232. [https://doi.org/10.1016/0016-7037\(95\)00038-2](https://doi.org/10.1016/0016-7037(95)00038-2)
- Weyer, S., Munker, C., Mezger, K., 2003. Nb/Ta, Zr/Hf and REE in the depleted mantle: implications for the differentiation history of the crust-mantle system. *Earth and Planetary Science Letters* 205 (3-4), 309-324. [https://doi.org/10.1016/S0012-821X\(02\)01059-2](https://doi.org/10.1016/S0012-821X(02)01059-2)
- Whalen, J.B., Currie, K.L., Chappell, B.W., 1987. A-type granites: geochemical characteristics, discrimination and petrogenesis. *Contributions to Mineralogy and Petrology* 95 (4), 407-419. <https://doi.org/10.1007/BF00402202>
- Whalen, J.B., McNicoll, V.J., Staal, C.R., Lissenberg, C.J., Longstaffe, F.J., Jenner, G.A., Breeman, O., 2006. Spatial, temporal, and geochemical characteristics of Silurian collision-zone magmatism, Newfoundland Appalachians, an example of a rapidly evolving magmatic system related to slab break-off. *Lithos* 89 (3-4), 377-404. <https://doi.org/10.1016/j.lithos.2005.12.011>
- Wilson, M., 1989. *Igneous Petrogenesis A Global Tectonic Approach*. Springer Dordrecht, 466p. <https://doi.org/10.1007/978-1-4020-6788-4>
- Wilson, M., 1994. *Igneous Petrogenesis*. Chapman & Hall, London, 466 pp.
- Winchester, J.A., Floyd, P.A., 1977. Geochemical discrimination of different magma series and their differentiation products using immobile elements. *Chemical geology* 20, 325-343. [https://doi.org/10.1016/0009-2541\(77\)90057-2](https://doi.org/10.1016/0009-2541(77)90057-2)
- Zartman, R.E., and Doe, B.R., 1981. Plumbotectonics- The model. *Tectonophysics* 75 (1-2), 135-162. [https://doi.org/10.1016/0040-1951\(81\)90213-4](https://doi.org/10.1016/0040-1951(81)90213-4)